Journal Pre-proofs

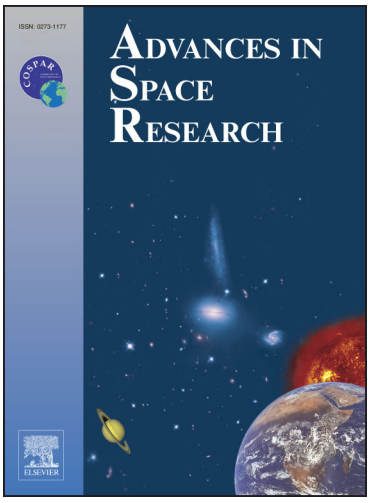

Energy spectra of abundant cosmic-ray nuclei in the NUCLEON experiment

V. Grebenyuk, D. Karmanov, I. Kovalev, I. Kudryashov, A. Kurganov, A. Panov, D. Podorozhny, A. Tkachenko, L. Tkachev, A. Turundaevskiy, O. Vasiliev, A. Voronin

PII: S0273-1177(19)30737-9
DOI: https://doi.org/10.1016/j.asr.2019.10.004
Reference: JASR 14484

To appear in: *Advances in Space Research*

Received Date: 5 December 2018
Revised Date: 30 September 2019
Accepted Date: 1 October 2019

Please cite this article as: Grebenyuk, V., Karmanov, D., Kovalev, I., Kudryashov, I., Kurganov, A., Panov, A., Podorozhny, D., Tkachenko, A., Tkachev, L., Turundaevskiy, A., Vasiliev, O., Voronin, A., Energy spectra of abundant cosmic-ray nuclei in the NUCLEON experiment, *Advances in Space Research* (2019), doi: https://doi.org/10.1016/j.asr.2019.10.004

Energy spectra of abundant cosmic-ray nuclei in the NUCLEON experiment

V.Grebenyuk[ab], D.Karmanov[c], I.Kovalev[c], I.Kudryashov[c], A.Kurganov[c], A.Panov[c], D.Podorozhny[c], A.Tkachenko[ad], L.Tkachev[ab], A.Turundaevskiy[c], O.Vasiliev[c], A.Voronin[c]

[a] *Joint Institute for Nuclear Research, Dubna, 141980, Russia*

[b] *Dubna State University, Dubna, 141980, Russia*

[c] *Skobeltsyn Institute of Nuclear Physics, Moscow State University, Moscow, 119991, Russia*

[d] *Bogolubov Institute for Theoretical Physics, Kiev, 03680, Ukraine*

Abstract

The NUCLEON satellite experiment is designed to directly investigate the energy spectra of cosmic-ray nuclei and the chemical composition (Z=1−30) in the energy range of 2–500 TeV. The experimental results are presented, including the energy spectra of different abundant nuclei measured using the new Kinematic Lightweight Energy Meter (KLEM) technique. The primary energy is reconstructed by registration of spatial density of the secondary particles. The particles are generated by the first hadronic inelastic interaction in a carbon target. Then additional particles are produced in a thin tungsten converter, by electromagnetic and hadronic interactions. The deconvolution of spectra was peformed. Statistical errors were presented.

Keywords: cosmic ray; spectrum; direct measurements

1.Introduction

The “knee” energy range - 10^{14} - 10^{16} eV - is a crucial region for the understanding of cosmic rays, acceleration and propagation in the interstellar medium. It is important to obtain more data with elemental resolution.

There are no direct measurements of cosmic ray nuclei spectra in the "knee" energy range. The main information about cosmic ray nuclei at 10^{12} - 10^{14} eV has been obtained by balloon (ATIC (Ahn et al., 2006, Panov et al., 2006), CREAM (Yoon et al., 2011, 2017, Ahn et al., 2009), TRACER (Obermeier et al., 2011)) and satellite (AMS02 (Aguilar et al., 2015a, 2015b, 2017, 2018a, 2018b) for lower energies, SOKOL (Ivanenko et al., 1993)) experiments. The CALET (Brogi et al., 2016) and ISS-CREAM (Seo et al., 2014) experiments are performed onboard ISS now. The DAMPE experiment (Wu et al., 2016) has also been realised. However, additional direct measurements at energies of up to 1000 TeV are necessary.

The NUCLEON satellite experiment is designed to directly investigate, above the atmosphere, the energy spectra of cosmic-ray nuclei and the chemical composition from 2 to more than 500 TeV (before the "knee"). The highest measured energy is equal to 900 TeV.

2. **The NUCLEON design**

The NUCLEON device (Atkin et al., 2015a, Vasiliev et al., 2014, Bulatov et al., 2010, Voronin et al., 2007a, 2007b, Podorozhnyi et al., 2007) was designed and produced by the collaboration of SINP MSU (the main investigator), JINR (Dubna) and a number of other Russian scientific and industrial centers. Currently, it is placed on board the RESURS-P №2 satellite. The spacecraft's orbit is a Sun-synchronous one, with an inclination of 97.276° and a middle altitude of 475 km. The satellite was launched on 26 December, 2014.

Scientific objectives and detection techniques determined the detector design. The general composition of the NUCLEON apparatus is presented in fig. 1.

The new Kinematic Lightweight Energy Meter (KLEM) technique was applied. The primary energy is reconstructed by registration of spatial density of the secondary particles. The particles are generated by the first hadronic inelastic interaction in a carbon target. The equivalent thickness of the carbon target is equal to 0.23 proton interaction lengths (10 cm).

Additional particles are produced in thin tungsten converter by electromagnetic and hadronic interactions. The spatial density of the secondary particles is measured by silicon microstrip detectors.

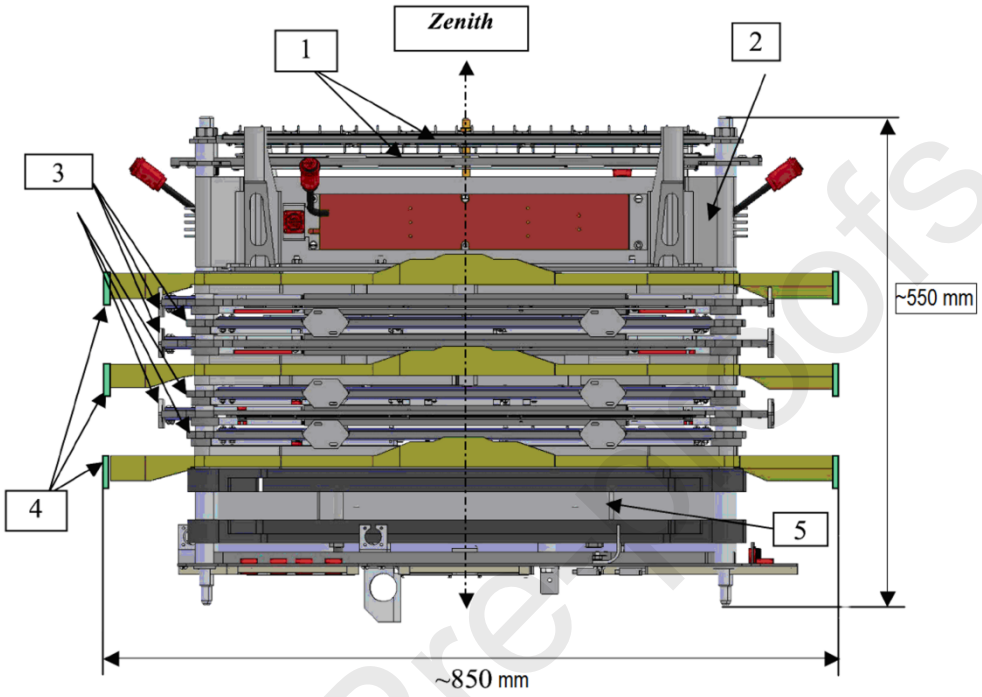

Figure 1: Cross sectional simplified layout of NUCLEON experiment scientifc equipment. (1) - two pairs of charge measurement system planes; (2) - carbon target; (3) - 6 planes of energy measurement system utilizing the KLEM technique; (4) - 3 double trigger system planes; (5) - calorimeter.

The NUCLEON apparatus includes different units based on silicon and scintillator detectors. The charge measurement system consists of 4 pad silicon detectors layers. The KLEM energy measurement system includes 6 silicon microstrip detectors interleaved with thin tungsten layers. There are six layers of plastic scintillator detectors of 0.75 cm thickness in the trigger system. They generate necessary trigger signals for the KLEM system. Each of the trigger planes consists of 16 scintillator strips. The light signals from the strips are collected by wave-length shifting (WLS) fibres to PMTs. The calorimeter also includes 6 silicon microstrip detectors.

The total weight of the device is about 375 kg. Power consumption is less than 175 W. The dimensions of the instrument are as follows: length, 85 cm; width, 85 cm ; height, 55 cm.

The effective geometric factor is more than 0.2 m^2sr for the KLEM system and nearly 0.06 m^2sr for the calorimeter. The surface area of the device is equal to 0.25 m^2. The charge measurement system provides a resolution of 0.15–0.20 charge units.

The set of data obtained by all detectors can be considered as the image of the event. An event example is presented in fig. 2. The reconstructed trajectory crosses charge detectors (1), KLEM system silicon microstripe detectors (3), and calorimeter silicon microstripe detectors (5). We can see a projection of the cascade in the device.

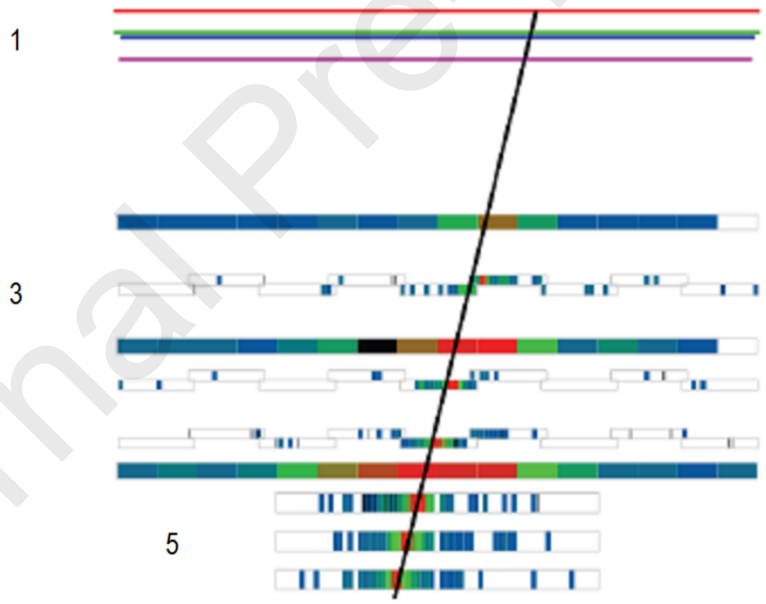

Figure 2. The image of the event. The boron nucleus with energy ~8 TeV initialized the shower. (1) - two pairs of charge measurement system planes; (3) - 6 planes of energy measurement system utilizing the KLEM technique; (5) - calorimeter. The color scales are relative. These scales are various for different detector planes.

3. The KLEM technique

A new energy measurement method KLEM was proposed in (Bashindzhagyan et al., 2005, Podorozhnyi et al., 2005, Korotkova et al., 2002, Adams et al., 2001,

Adams et al., 2000). The technique can be used over a wide range of energies (10^{11}–10^{16} eV) and gives an energy resolution of 70% or better, according to simulation results (Bulatov et al., 2010, Voronin et al., 2007b, Podorozhnyi et al., 2007, Postnikov et al., 2002).

We have considerably improved a kinematical method. The simple kinematical method for the determination of the primary particle energy proposed by Castagnoli (Castagnoli et al., 1953) gives large errors between 100% and 200%. To overcome this problem, a combined method was proposed. This is based, on the one hand, on the measurements of spatial density of not only charged secondaries, but also neutral ones. On the other hand, a measuring technique at the data processing stage is proposed, which allows for an increased contribution of faster secondaries to the energy determination, and eliminates that of slower ones.

The primary energy is reconstructed by registration of spatial density of the secondary particles. The new particles are generated by the first hadronic inelastic interaction in a carbon target. Then, additional particles are produced in the thin tungsten converter by electromagnetic and hadronic interactions. The main difference between the proposed KLEM method and ionisation calorimeters is that the KLEM technique does not need heavy absorbers for the shower measurement. Thus, it is possible to design relatively light cosmic-ray detectors with a large geometric factor.

We use the S-estimator for the energy determination:

$$S = \sum_{i=1}^{N} \eta_i^2$$

where summation is over all N-secondaries detected after the converter, $\eta_i = -\ln \mathrm{tg}\theta_i/2 \approx -\ln(r_i/2H)$, θ_i is the angle between the shower axis and secondary particle direction, r_i is the distance from the shower axis for all position-sensitive detector layers located after the converter, and H is the distance from the interaction point in the target. The estimator depends on the angular distribution of secondaries. The number of secondaries with minimal angles is more sensitive to the Lorentz factor of the primary particle than the total multiplicity. The squaring

increases the contribution of these particles. For the real apparatus we apply H determined as the distance from the middle of the target to the detector layer.

For example, the value of $\ln^2(2H/x)$ is equal to 48.4 for the middle of the target (H=255 mm) and 45.4 for the low boundary of the target (H=204 mm). Thus, the maximal systematic deviation is near 6%. The direct simulation shows that the rms deviation of reconstructed energy (see below) increased from 70% (for true interaction point) to 70.2%. On the one hand, the S-estimator characterises the distribution of secondaries on emission angles as being sensitive to the Lorentz-factor of the primary particle. On the other hand, S is proportional to the multiplicity of secondaries produced in the target and multiplied in the converter. The contribution of slow neutrals is eliminated by the squaring of η. Simulations showed the simple semi-empirical power law energy dependence for S (Adams et al., 2001).

The perpendicular projections x_i and y_i can be used instead of the distance r_i. This allows us to exploit microstrip silicon detectors for spatial measurements. The microstrip detectors can register many charged particles per strip. The signal is proportional to the strip ionisation or the number of single-charged particles. Thus, the S-estimator is defined as:

$$S = \sum_k I_k \ln^2(2H/x_k)$$

where x_k is a distance between the shower axis and the strip k, I_k is a signal in the strip k.

The simple semi-empirical power law $\langle S(E) \rangle \sim E^{0.7\text{-}0.8}$ dependence of the energy per nucleon was obtained.

The above-mentioned squaring and multiplication of secondaries in the converter make energy dependence steeper than for multiplicity in the first interaction. For incident nucleus with mass number A not all of the nucleons interact with the target carbon nucleus. Therefore, the multiplicity of secondaries is not proportional to A but the angular distribution of secondaries is similar to the

distribution for one proton. The $\langle S(E) \rangle$ dependence is similar for different types of primary nuclei in the wide energy range.

The simulation and beam test results were compared for Minimum Ionizing Particles (MIPs) detection to elaborate absolete energy scale.

We used the standard scintillators and sensors with known characteristics. The special read-out chip with high dynamic range was elaborated (Atkin et al., 2015c). The response of energy measurement system was tested by means of accelerator pion beams. The absolete energy scale was tested. Accelerator calibration tests are described in Sec.5.

4. Simulations

4.1. The simulation of the energy measurement system.

Isotropic fluxes of protons, and helium, carbon, sulphur and iron nuclei were simulated. For constant statistical accuracy on all studied energy ranges (100 GeV — 1000 TeV), a uniform logarithmic distribution on energy was simulated dN/d(lnE)=const. Earlier preliminary simulation showed applicability of the KLEM technique up to 10000 TeV. The main part of statistics is expected at energies 2-500 TeV. The signal in the scintillator and silicon detectors was considered proportional to the energy deposit in the corresponding volume. The detectors applied in the NUCLEON experiment were tested and calibrated by accelerator beams. Algorithms are completely identical to processing of the simulated and experimental databanks. Selection by trigger conditions and reconstruction of the primary particle track were reproduced. For selected events, an optimisation of the KLEM technique was performed. The calibration dependencies were calculated.

The practical applicability of the proposed KLEM energy measurement technique was estimated using the results of the simulation, employing the GEANT 3.21 (Brun, 1983) software package complemented by the QGSJET (Kalmykov et al., 1997, Batkov et al., 2011) nuclear interaction generator to describe high-energy hadron–nucleus and nucleus–nucleus interactions.

4.2. The energy reconstruction for different components

For the results of the simulation analysis the following main assumptions were applied.

First, a power-law dependence of the reconstructed energy on the estimator S, defined earlier, was assumed.

$$E_{rec} = aS^b$$

Second, the distribution function on the reconstructed energy does not depend on primary energy, only on the ratio of the reconstructed and primary energy $F(E_{rec}/E)$.

Let us designate $k = E_{rec}/E$

We know that cosmic-ray spectra are close to power law.

$$\frac{dN}{dE} = AE^{-(\gamma+1)}$$

At the given reconstructed energy:

$$E = E_{rec}/k$$

$< k >= 1$ for the power energy spectrum.

Therefore, the following equations are obtained:

$$\frac{dN}{dk} = AE_{rec}^{-\gamma}k^{\gamma}$$

$$< k >= \frac{\sum k_i^{\gamma+1}}{\sum k_i^{\gamma}} = 1$$

We obtained for a simulated event with energy E_i

$$k_i = \frac{aS_i^b}{E_i}$$

As a result, we receive the formula for a:

$$a = \frac{\sum (S_i^b/E_i)^{\gamma}}{\sum (S_i^b/E_i)^{\gamma+1}}$$

By means of the ordinary least squares method, the b values for different components were received from simulated databanks. The a values were calculated according to the formula received above. It is necessary to calculate the

unbiased value of energy for the power spectrum. In practice, the more convenient parameter, $a_{2,}$ was applied:

$$E_{rec} = a_2 (S \cdot 10^{-5})^b$$

The values of a_2 and b are presented in Table 1.

Table 1. Energy reconstruction parameters

Projectile nucleus	a_2 GeV	b
p	1651±82	1.357±0.009
He	2556±125	1.274±0.008
C	3514±199	1.180±0.009
S	4163±230	1.141±0.008
Fe	4362±195	1.119±0.007

The simulation results (S vs E) are presented in fig.3 for protons and carbon nuclei.

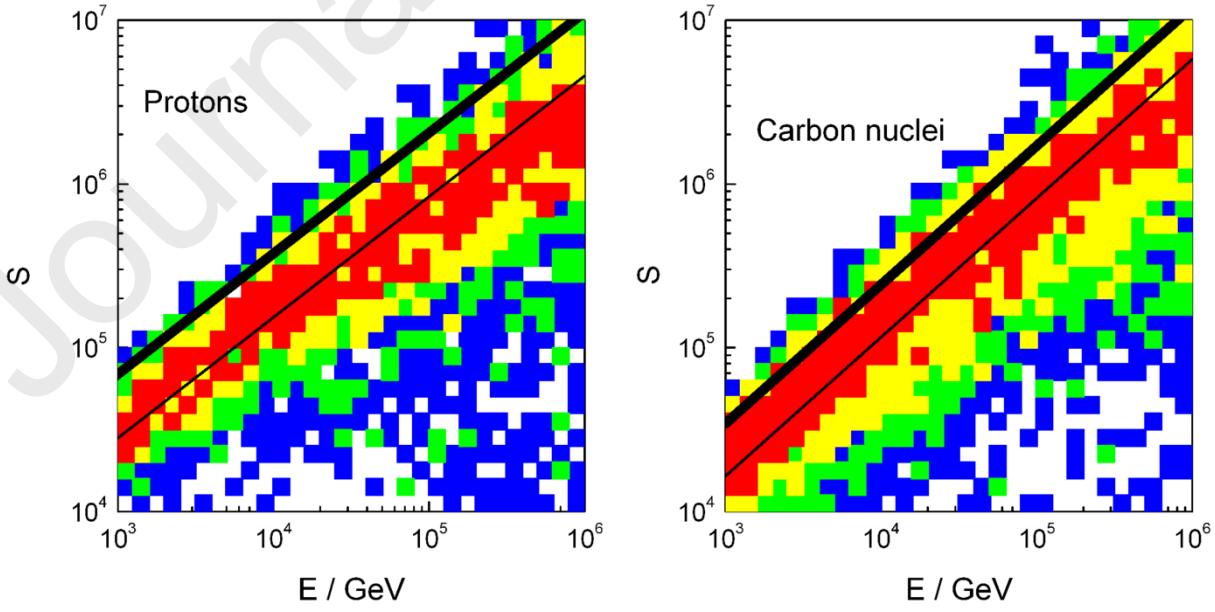

Figure 3. Simulation results. S vs E for protons and carbon nuclei. The fit (thick line) is shifted according to the power spectrum ($\gamma = 1.6$). The thin line corresponds to simple fit of data.

The primary particles were generated with uniform energy distribution in logarithmic scale by the simulation. The thin line in fig.3 is the power fit of these data. However the real cosmic-ray energy spectra are close to power law spectra. Thus it is necessary to apply event weights according to expected energy spectra. The thick line corresponds to the fit obtained with event weights for the power spectrum. The fit lines deviation from the peak is caused by the power spectrum correction. According to above-mentioned formula the parameter a is equal to $a = \frac{\sum (S_i^b / E_i)^\gamma}{\sum (S_i^b / E_i)^{\gamma+1}}$ for the power spectrum ($\gamma = 1.6$). The simple fit for the simulated databank corresponds to $a = \frac{N}{\sum (S_i^b / E_i)}$.

The dependence of the energy resolution on energy is shown in fig.4 for different projectile nuclei according to parameters from Table 1, taking into account power shape of cosmic-ray spectra. The reconstructed energy distribution is a convolution of distributions at fixed energies and shape of spectrum. Thus, the resolution can depend on a spectral exponent.

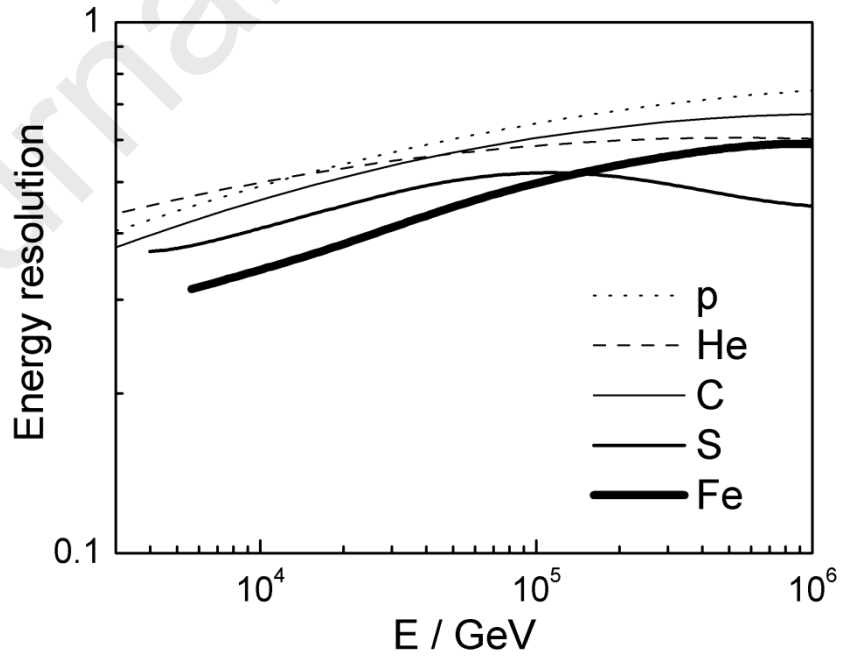

Figure 4. Energy resolution dependence on energy (simulation)

4.3. The registration efficiency for different nuclei

At the given algorithm of energy reconstruction, the registration efficiency can be determined as the ratio of reconstructed and primary energy spectra by simulation results. In practice, it is a combined parameter. Different effects influencing the registration efficiency were not determined separately because they were automatically taken into account by the simulation.

The registration efficiency depends on the probability of interaction of the corresponding particle in the device, trigger conditions, and also error in the energy measurements. Accounting for energy dependence of registration efficiency is necessary for the solution of the problem of deconvolution, i.e. a correct reconstruction of energy spectra.

At low energies, fragments of primary, heavy nuclei interacting in the carbon target can imitate a particle with energy near 1-3 TeV. Moreover, there are other threshold effects. It allows for reconstruction of energy spectra only at energies more than 3-5 TeV. The energy dependences of the registration efficiency calculated by simulation results, according to the definition given above, are presented in fig. 5. The registration efficiencies for light nuclei are low because of the small interaction probability in the carbon target and low multiplicity of secondary particles generated by the first inelastic interaction.The calculated dependences are rather smooth. It allows the use of interpolation of energy and a charge for various nuclei of cosmic rays.

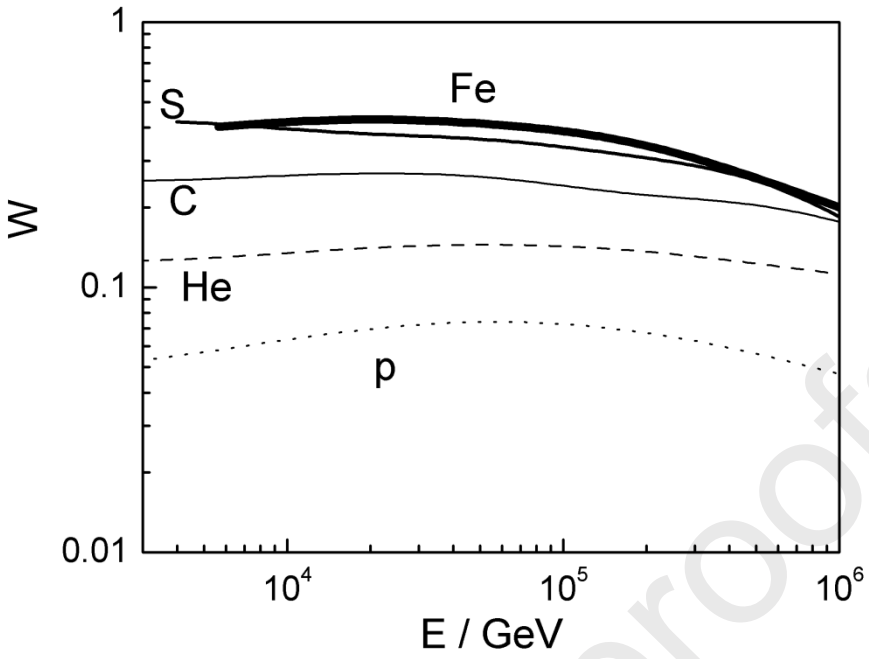

Figure 5. The registration efficency calculated for power spectra according to trigger conditions (Atkin et al., 2017a)

5. Beam tests of the energy measurement system.

Tests of the KLEM method with NUCLEON prototypes were performed at the pion 100–350 GeV beams of the SPS accelerator at CERN (Bulatov et al., 2010, Voronin et al., 2007b). The procedure for reconstructing the particle energy uses the theoretical calibration dependence of parameter $S(E)$. The calibration cureves for high energy protons and carbon nuclei are presented in Fig.3. Based on the simulation data, the calibration dependence $<S(E)>$ estimator of energy was plotted and the power law index was found to be 0.75.

In a second step, the NUCLEON flight model was tested. Pion data were obtained for 150 and 350 GeV. The coordinates of the shower axes were determined by the microstrip detector signals. The S values were calculated for every selected event.

Energy dependence S(E) is presented in fig.6. The data were obtained for the pion beam of 2013 (squares) and the previous tests in 2008 (circles) (Atkin et al., 2015a). The curves were obtained by simulation for different trigger criteria.

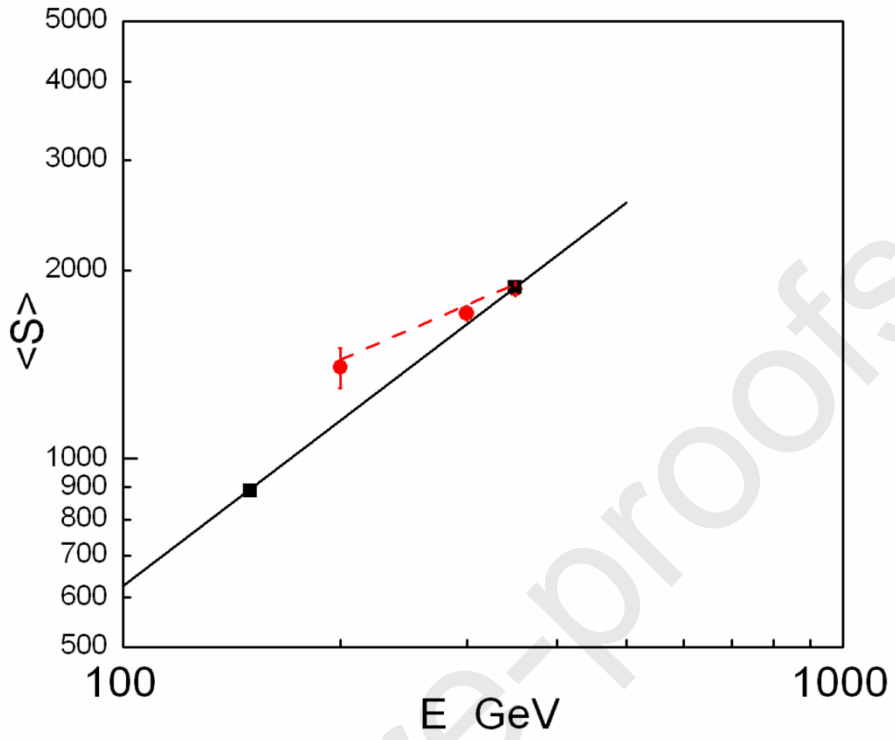

Figure 6. The calibration energy dependence S(E) for pions. The points were obtained for the pion beam of 2013 (squares) and the previous tests in 2008 (circles) (Atkin et al., 2015a). The curves was obtained by simulation for different trigger criteria (the solid line corresponds to the test of 2013, the dashed line corresponds to the test of 2008).

The normalised distributions of the reconstructed energy for primary pions with energies of 150 (thin line) and 350 GeV (thick line) are shown in fig. 7 (Atkin et al., 2015a). The rms deviation to primary energy ratio is equal to 0.53 for 150 GeV and 0.63 for 350 GeV. The asymmetry of the distributions is determined by the asymmetry of multiplicity distributions for hadron interactions.

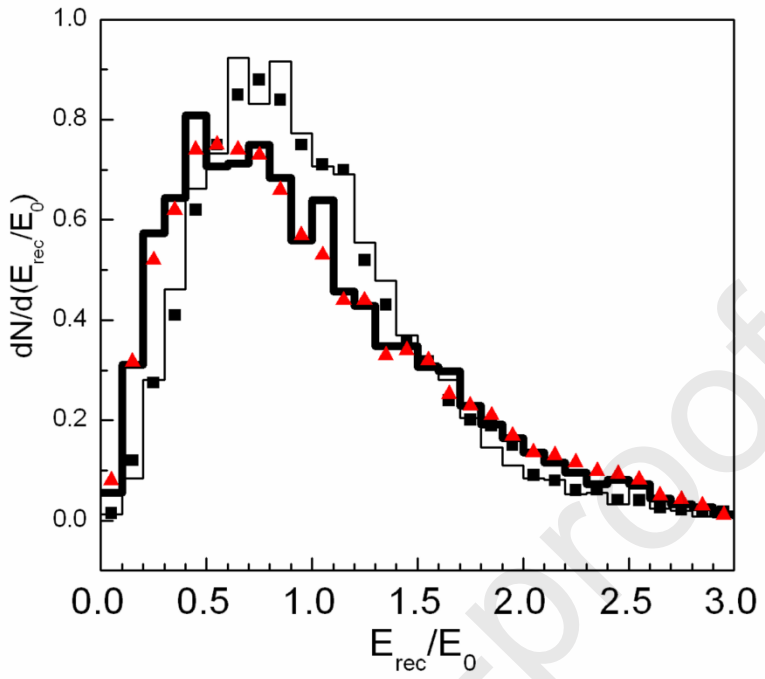

Figure 7. Normalized reconstructed energy distributions for pion beams of 150 GeV (thin line, squares) and 350 GeV (thick line, triangles) (Atkin et al., 2015a). Squares and triangles correspond to simulation results.

6. The space experiment results

6.1. Event selection and charge measurements

The trigger system based on scintillator detectors provided registration of events with energy more than several hundred GeV. The top detector trigger condition was aimed to select events with the first hadronic interaction in the carbon target. Trigger thresholds were changed during the flight. More detailed selection were done by off-line software.

Processing of data obtained by the satellite experiment consists of several stages.

At the first stage, the trajectory of the particle is analysed. Maxima of the spatial distribution of ionisation are searched for each microstrip detector layer of

the energy measurement system. It is supposed that these maxima correspond to track cross points with the detector layers. On these points the axis is reconstructed by Ordinary Least Squares. Events where the axis is located within a fiducial acceptance are selected.

For each layer of the charge measurement system the cross point with this particle trajectory is reconstructed. Around this point, (taking into account possible error), coordinates of pads through which a primary particle can pass are determined. The signals from these pads are compared and the largest amplitude is selected.

Calibrations are necessary for transition from the registered signal amplitude to the charge value. At the first stage, the beam tests results were used. Changes for each channel were considered by means of on-board calibration.

The initial calibrations were applied to obtain the first level charge distributions with charge errors near 0.3-0.5. Further analysis showed that the dispersion of characteristics of the various detectors of the charge measurement system is the main reason for a high error.

After the registration of rather large statistics (half a year of the experiment), charge distributions were successfully received separately for each of 256 charge measurement system detectors.

For each such distribution, the reference peaks from the most abundant nuclei, e.g. protons, helium, carbon, oxygen and iron are allocated (Z=1,2,6,8,26). The additional calibration for each detector is based on these peak values.

The charge spectra of the four detectors were matched using the rank statistics method (Voronin et al., 2007a). For each recorded event four charges were measured by the four detectors and arranged in ascending order (regardless of the detector to which a particular charge corresponded). The next step was to determine the charge that is second in magnitude, and this value was used as the estimate for the charge.

Thus, the charge distributions with high resolution (0.15-0.20 for different nuclei) were obtained (fig.8). The small offset of the charge peaks (Z>14) is

caused by nonlinearity of electronics. This effect was taken into account by elemental selection.

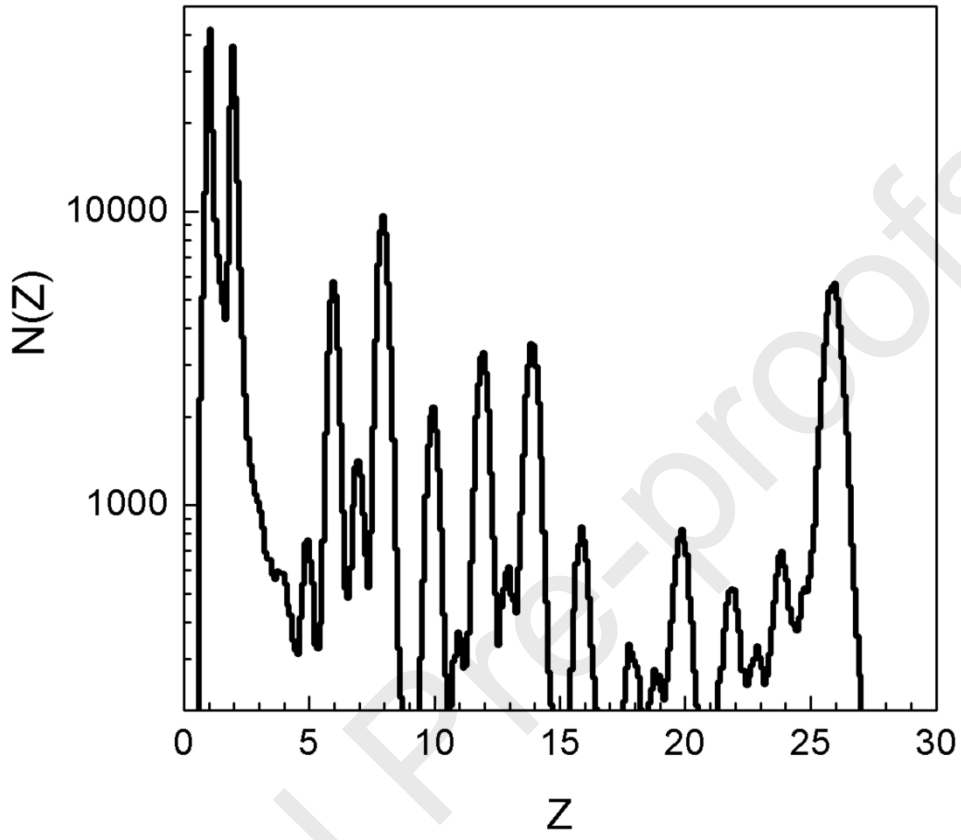

Figure 8. Charge distribution for all events registered according to trigger criteria (energies more than ~1 TeV) for two years (2015-2016).

The calorimeter data were applied to reconstruct tracks for approximately fourth part of events. We selected events with charge signal $Z_i - 0.5 < Z < Z_i + 0.5$ as nuclei with charge Z_i . There is negligible contamination (lower than 1%) of abundant nuclei for this condition. The proton contamination to the helium spectrum is evaluated as 1.5% according to simulation results. The helium contamination to protons is less than 1%. The additional strict selection is necessary for the analysis of rare nuclei.

6.2. Energy spectra reconstruction

By deconvolution, both energy dependence of the S-estimator and energy dependence of the registration efficiency are considered.

The differential flux of particle species is given by

$$\frac{dN}{d\ln E} = \frac{1}{\Gamma w W} \frac{\Delta N}{\Delta(\ln E)\Delta T}$$

In this formula, Γ is the geometrical factor, w is fraction of the live time, W is the registration efficiency, ΔN is the number of registered nuclei, Δ(lnE) is the bin width, ΔT is the exposure time.

The Γ and W parameters were determined by Monte Carlo simulations (see 4.3). Nonlinear function E(S) allows to use for deconvolution simple diagonal matrix with ΓW matrix element for every energy bins. This simple approach was used as a first approximation to reconstruct energy spectra. Later the more detailed deconvolution method was elaborated.

Examples of artificial spectra simulated and reconstructed by the above described method energy spectra are presented in fig.9. Both simple power spectrum and a spectrum with a break can be reconstructed.

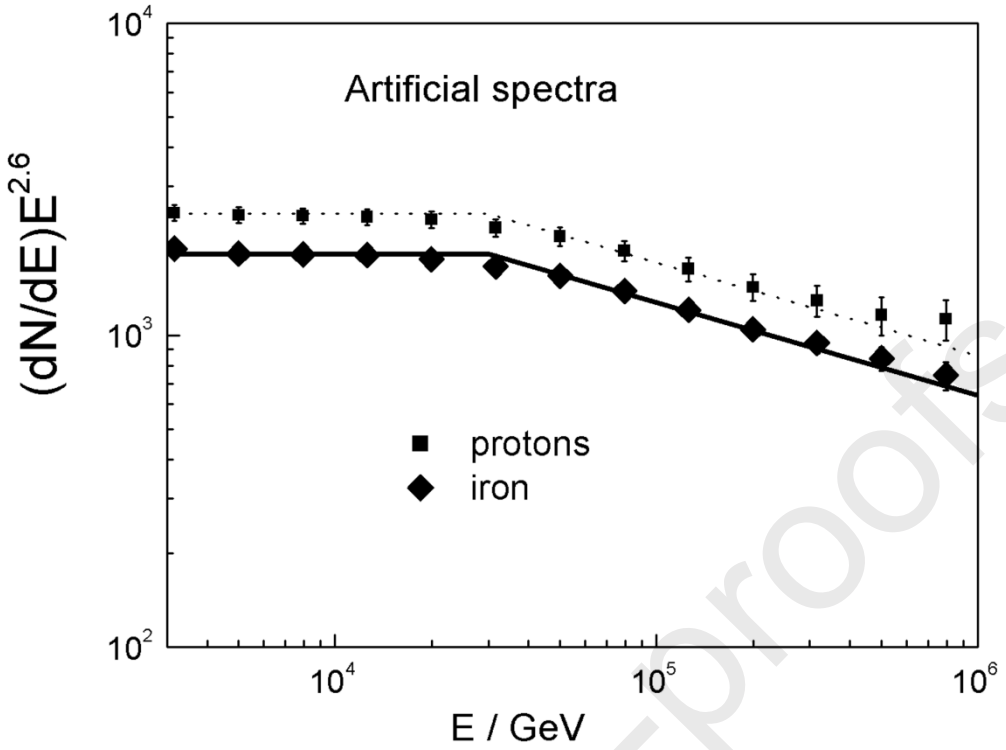

Figure 9. The simulated (lines) and reconstructed (points) energy spectra

Possible systematic uncertainties can be caused by different mechanisms. Electronic noise in silicon detectors can cause systematic uncertainty in the energy resolution. Low signals in detectors with magnitude less than 0.5 mip were neglected, in order to decrease this effect. The beam tests and simulation results were processed. The simulated and experimental reconstructed energy distributions are very close. The difference of mean reconstructed energies is near 4.6% (Voronin et al., 2007b). It is significantly less than physical fluctuations.

Any uncertainty in energy measurements results in a systematic shift in the reconstructed flux intensity. This shift depends on the energy resolution too.

The registration efficiency was calculated as a generalized parameter and different effects were taken into account, including the resolution energy dependence. Thus the correction by the calculated registration efficiency allows restoration of energy spectra.

Preliminarily, the systematic uncertainty of the flux depends on determinaton of the effective acceptance and the calibration of S. We evaluated these effects by variation of parameters. The systematic uncertainty of the effective acceptance is evaluated as 0.03 for heavy nuclei and 0.06 for protons due to acceptance dependence on the spectral exponent. The calibration of S is determined by periodical measurements of amplification factors for every channels. The systematic uncertainty of the calibration of S is equal to 0.0005.

We continue the analysis of systematic errors caused by simulation uncertanities and plan to publish a separate paper on this subject.

The additional test of the KLEM technique is comparison of reconstructed spectra with spectra obtained by traditional ionisation calorimeter (Atkin et al., 2015b, 2017a, 2017b, 2017c).

The both methods are used for the cross-calibration. The energy was determined by two methods (E_{KLEM} and E_{IC}) for different events. The Pearson product-moment correlation coefficient for E_{KLEM} and E_{IC} is equal to 0.82 (Atkin et al., 2017b). The distribution of ratio E_{KLEM}/E_{IC} obtained by the space experiment is presented in fig.10 for primary protons and helium nuclei.

Energy values determined by two methods are close. The middle ratio E_{KLEM}/E_{IC} is equal to 0.87. The difference of methods is significantly less than measurement errors.

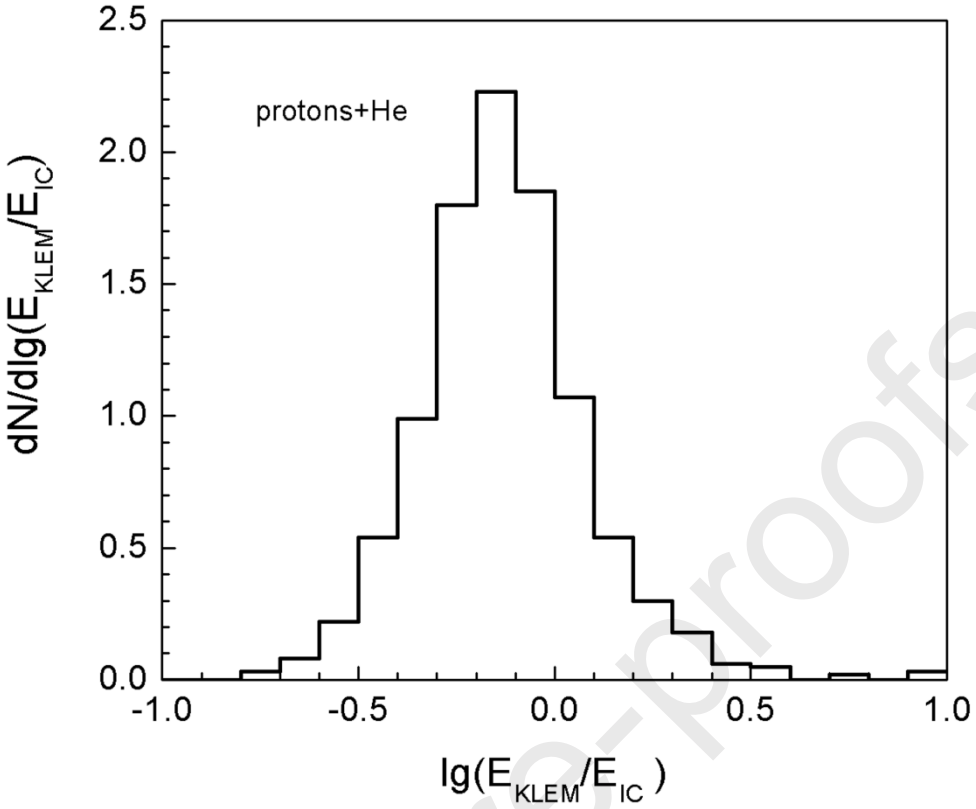

Figure 10. The distribution of ratio E_{KLEM}/E_{IC}

The energy spectra of different components of cosmic rays were reconstructed by means of the simple diagonal matrix. The proton and helium spectra were reconstructed by means of deconvolution with the Tikhonov regularization. Howewer this method is not reliable for the low statistics (Atkin et al., 2019). The all particles' energy spectrum (Atkin et al., 2015b, 2017b) was also reconstructed. The spectra of abundant components (protons, helium, carbon, oxygen, neon, magnesium, silicon, iron nuclei) were published in (Atkin et al., 2019).
Later we applied the detailed deconvolution for all events registered for three years (2015-2017). The deconvolution allows to correct spectra to bin-to-bin migration effects. The corrected numbers of events in the energy bin *i* were calculated by the relation $\Delta N_{cor,i} = \sum_j P_{ij} \Delta N_j$ (Yoon et al., 2011).

Thus the statistical errors of deconvoluted spectra were calculates as

$$\sigma(\Delta N_{cor,i}) = \sqrt{\sum_j P_{ij}^2 \Delta N_j}$$

The statistical errors are less than without the deconvolution but these errors are correlated because of summation of different values ΔN_j.

The matrix elements P_{ij} were calculated by means of Monte-Carlo simulation for the power spectrum with integral exponent $\gamma = 1.6$.

We evaluated the systematic uncertaities caused by different reasons. The effect caused by low energy resolution was investigated by the additional Monte-Carlo simulation. This simulation was performed for the every obtained spectrum of registered energies ΔN_j. The primary energy distribution was simulated according to the matrix P_{ij}. Thus we evaluated these errors depending on statistics.

The uncertainty of energy response can be related to the uncertainty of the simulation. We compared simulation results obtained by GEANT 3.21 including QGSJET and by GEANT4. The difference between values of reconstructed energy for the same value of the S estimator is near 6%. We assumed this value as the estimation of the energy determination systematic error.

The uncertainty of the geometric factor caused by errors of the track reconstruction. We applied the Monte-Carlo simulation to evaluate this effect. We took into account not working strips and physical fluctuations of showers in the NUCLEON device. Thus the uncertainty of the geometric factor is evaluated as 5.6%.

The statistical and systematic errors were calculated. Obtained spectra are presented in figs. 11-18. The spectra for the KLEM technique and the ionization calorimeter (IC) (Atkin et al., 2017a) are shown. The statistcal errors and boundaries of total errors area are presented.

The difference between the deconvoluted spectra and spectra obtained by other methods can be considered as systematics too. Thus the obtained systematic errors should be considered as lower bound.

The results are presented in the Table 2 too. This table includes values of $\Delta N_{cor,i} = \sum_j P_{ij} \Delta N_j$ corresponded to the unfolded flux of cosmic ray components.

These values are results of summing up of events numbers ΔN_j for all bins with different weights. Null-event bins are taken into account too. The null-event bin effect is suppressed by bins with high statistics.

We present values $\Delta N_{cor,i}$ only for bins with $\Delta N \geq 2$. The null-event bins are only at high energies, $j > i$. The corresponding values of coefficients P_{ij} are significantly less than P_{ii}. The numerous events of bins with $j < i$ make a contribution to the bin i too. Therefore the influence of null-event bins on $\Delta N_{cor,i}$ and $\sigma(\Delta N_{cor,i})$ is very small. For example, we analyzed the proton spectrum. The artificial increase of the value ΔN_j from 0 to 1 increases the value $\Delta N_{cor,i}$ less than by 2%.

The main errors caused by the low energy resolution were taken into account by means of the additional Monte-Carlo simulation as part of systematic uncerainties (see above).

Table 2. Deconvoluted energy spectra obtained by the NUCLEON experiment

Particle	Energy, GeV	Flux (m2 sr s GeV)$^{-1}$	Statistical error	Systematic error	ΔN_{cor}
Protons	$3.16 \cdot 10^3$	$3.62 \cdot 10^{-6}$	$1.99 \cdot 10^{-8}$	$4.07 \cdot 10^{-7}$	4920.9
	$5.01 \cdot 10^3$	$1.11 \cdot 10^{-6}$	$8.16 \cdot 10^{-9}$	$1.26 \cdot 10^{-7}$	2866.0
	$7.94 \cdot 10^3$	$3.51 \cdot 10^{-7}$	$3.55 \cdot 10^{-9}$	$4.01 \cdot 10^{-8}$	1432.7
	$1.26 \cdot 10^4$	$1.09 \cdot 10^{-7}$	$1.40 \cdot 10^{-9}$	$1.29 \cdot 10^{-8}$	822.5
	$2.00 \cdot 10^4$	$3.46 \cdot 10^{-8}$	$6.21 \cdot 10^{-10}$	$4.25 \cdot 10^{-9}$	412.9
	$3.16 \cdot 10^4$	$1.05 \cdot 10^{-8}$	$2.23 \cdot 10^{-10}$	$1.44 \cdot 10^{-9}$	217.1
	$5.01 \cdot 10^4$	$3.15 \cdot 10^{-9}$	$9.10 \cdot 10^{-11}$	$5.00 \cdot 10^{-10}$	103.5
	$7.94 \cdot 10^4$	$9.13 \cdot 10^{-10}$	$3.22 \cdot 10^{-11}$	$1.82 \cdot 10^{-10}$	52.3
	$1.26 \cdot 10^5$	$2.63 \cdot 10^{-10}$	$1.35 \cdot 10^{-11}$	$7.58 \cdot 10^{-11}$	24.1
	$2.00 \cdot 10^5$	$7.48 \cdot 10^{-11}$	$4.78 \cdot 10^{-12}$	$2.62 \cdot 10^{-11}$	11.2

	$3.16•10^{3}$	$2.79•10^{-6}$	$1.43•10^{-8}$	$3.12•10^{-7}$	7062.6
	$5.01•10^{3}$	$9.49•10^{-7}$	$6.24•10^{-9}$	$1.06•10^{-7}$	4114.6
	$7.94•10^{3}$	$3.28•10^{-7}$	$2.83•10^{-9}$	$3.70•10^{-8}$	2255.3
	$1.26•10^{4}$	$1.08•10^{-7}$	$1.14•10^{-9}$	$1.23•10^{-8}$	1235.1
	$2.00•10^{4}$	$3.61•10^{-8}$	$5.22•10^{-10}$	$4.22•10^{-9}$	654.7
	$3.16•10^{4}$	$1.14•10^{-8}$	$2.11•10^{-10}$	$1.41•10^{-9}$	384.4
	$5.01•10^{4}$	$3.64•10^{-9}$	$9.22•10^{-11}$	$4.80•10^{-10}$	194.0
	$7.94•10^{4}$	$1.09•10^{-9}$	$3.40•10^{-11}$	$1.70•10^{-10}$	92.1
	$1.26•10^{5}$	$3.26•10^{-10}$	$1.43•10^{-11}$	$6.21•10^{-11}$	43.9
	$2.00•10^{5}$	$9.68•10^{-11}$	$5.39•10^{-12}$	$2.52•10^{-11}$	21.6
	$3.16•10^{5}$	$2.74•10^{-11}$	$2.19•10^{-12}$	$9.57•10^{-12}$	9.8
	$5.01•10^{5}$	$8.07•10^{-12}$	$9.32•10^{-13}$	$4.01•10^{-12}$	4.8
	$7.94•10^{5}$	$2.31•10^{-12}$	$4.51•10^{-13}$	$1.54•10^{-12}$	2.2
He					
	$3.16•10^{3}$	$5.59•10^{-7}$	$5.56•10^{-9}$	$6.28•10^{-8}$	2248.7
	$5.01•10^{3}$	$1.91•10^{-7}$	$2.40•10^{-9}$	$2.18•10^{-8}$	1298.1
	$7.94•10^{3}$	$6.63•10^{-8}$	$1.09•10^{-9}$	$7.75•10^{-9}$	715.6
	$1.26•10^{4}$	$2.13•10^{-8}$	$4.59•10^{-10}$	$2.58•10^{-9}$	379.4
	$2.00•10^{4}$	$6.80•10^{-9}$	$1.92•10^{-10}$	$8.85•10^{-10}$	192.9
	$3.16•10^{4}$	$2.12•10^{-9}$	$7.58•10^{-11}$	$3.13•10^{-10}$	100.2
	$5.01•10^{4}$	$6.74•10^{-10}$	$3.56•10^{-11}$	$1.19•10^{-10}$	50.6
	$7.94•10^{4}$	$2.15•10^{-10}$	$1.47•10^{-11}$	$4.73•10^{-11}$	24.1
	$1.26•10^{5}$	$6.83•10^{-11}$	$6.92•10^{-12}$	$2.00•10^{-11}$	12.3
	$2.00•10^{5}$	$2.03•10^{-11}$	$2.52•10^{-12}$	$8.15•10^{-12}$	6.0
C					
	$5.01•10^{3}$	$2.76•10^{-7}$	$2.64•10^{-9}$	$3.17•10^{-8}$	1969.3
	$7.94•10^{3}$	$9.64•10^{-8}$	$1.23•10^{-9}$	$1.13•10^{-8}$	1091.0
	$1.26•10^{4}$	$3.22•10^{-8}$	$5.47•10^{-10}$	$3.89•10^{-9}$	596,5
	$2.00•10^{4}$	$1.05•10^{-8}$	$2.44•10^{-10}$	$1.33•10^{-9}$	309.8
	$3.16•10^{4}$	$3.24•10^{-9}$	$9.38•10^{-11}$	$4.59•10^{-10}$	158.1
	$5.01•10^{4}$	$9.99•10^{-10}$	$4.16•10^{-11}$	$1.61•10^{-10}$	77.5
	$7.94•10^{4}$	$3.08•10^{-10}$	$1.67•10^{-11}$	$6.19•10^{-11}$	36.1
	$1.26•10^{5}$	$9.47•10^{-11}$	$7.80•10^{-12}$	$2.46•10^{-11}$	17.7
	$2.00•10^{5}$	$2.83•10^{-11}$	$2.95•10^{-12}$	$1.04•10^{-11}$	8.6
O					

Ne	$5.01 \cdot 10^{3}$	$5.01 \cdot 10^{-8}$	$9.59 \cdot 10^{-10}$	$6.72 \cdot 10^{-9}$	374.3
	$7.94 \cdot 10^{3}$	$1.83 \cdot 10^{-8}$	$5.07 \cdot 10^{-10}$	$2.61 \cdot 10^{-9}$	215.9
	$1.26 \cdot 10^{4}$	$6.32 \cdot 10^{-9}$	$2.41 \cdot 10^{-10}$	$1.03 \cdot 10^{-9}$	121.6
	$2.00 \cdot 10^{4}$	$2.19 \cdot 10^{-9}$	$1.12 \cdot 10^{-10}$	$3.96 \cdot 10^{-10}$	66.9
	$3.16 \cdot 10^{4}$	$6.96 \cdot 10^{-10}$	$4.59 \cdot 10^{-11}$	$1.50 \cdot 10^{-10}$	35.0
	$5.01 \cdot 10^{4}$	$2.21 \cdot 10^{-10}$	$1.99 \cdot 10^{-11}$	$6.03 \cdot 10^{-11}$	17.7
	$7.94 \cdot 10^{4}$	$6.84 \cdot 10^{-11}$	$7.82 \cdot 10^{-12}$	$2.46 \cdot 10^{-11}$	8.3
	$1.26 \cdot 10^{5}$	$2.37 \cdot 10^{-11}$	$4.18 \cdot 10^{-12}$	$1.10 \cdot 10^{-11}$	4.6
	$2.00 \cdot 10^{5}$	$8.21 \cdot 10^{-12}$	$1.84 \cdot 10^{-12}$	$4.90 \cdot 10^{-12}$	2.6
Mg	$7.94 \cdot 10^{3}$	$2.35 \cdot 10^{-8}$	$5.80 \cdot 10^{-10}$	$3.26 \cdot 10^{-9}$	290.9
	$1.26 \cdot 10^{4}$	$8.27 \cdot 10^{-9}$	$2.63 \cdot 10^{-10}$	$1.20 \cdot 10^{-9}$	164.7
	$2.00 \cdot 10^{4}$	$2.84 \cdot 10^{-9}$	$1.26 \cdot 10^{-10}$	$4.69 \cdot 10^{-10}$	89.8
	$3.16 \cdot 10^{4}$	$8.94 \cdot 10^{-10}$	$4.99 \cdot 10^{-11}$	$1.76 \cdot 10^{-10}$	46.4
	$5.01 \cdot 10^{4}$	$2.75 \cdot 10^{-10}$	$2.23 \cdot 10^{-11}$	$6.81 \cdot 10^{-11}$	22.7
	$7.94 \cdot 10^{4}$	$8.19 \cdot 10^{-11}$	$8.37 \cdot 10^{-12}$	$2.67 \cdot 10^{-11}$	10.4
	$1.26 \cdot 10^{5}$	$2.33 \cdot 10^{-11}$	$3.41 \cdot 10^{-12}$	$1.08 \cdot 10^{-11}$	4.7
Si	$1.26 \cdot 10^{4}$	$8.27 \cdot 10^{-9}$	$2.84 \cdot 10^{-10}$	$1.18 \cdot 10^{-9}$	170.3
	$2.00 \cdot 10^{4}$	$3.08 \cdot 10^{-9}$	$1.39 \cdot 10^{-10}$	$4.69 \cdot 10^{-10}$	100.6
	$3.16 \cdot 10^{4}$	$1.02 \cdot 10^{-9}$	$5.59 \cdot 10^{-11}$	$1.86 \cdot 10^{-10}$	54.7
	$5.01 \cdot 10^{4}$	$3.51 \cdot 10^{-10}$	$2.65 \cdot 10^{-11}$	$7.53 \cdot 10^{-11}$	29.8
	$7.94 \cdot 10^{4}$	$1.09 \cdot 10^{-10}$	$1.04 \cdot 10^{-11}$	$3.18 \cdot 10^{-11}$	14.4
	$1.26 \cdot 10^{5}$	$3.34 \cdot 10^{-11}$	$4.51 \cdot 10^{-12}$	$1.31 \cdot 10^{-11}$	7.0
Fe	$1.26 \cdot 10^{4}$	$1.86 \cdot 10^{-8}$	$4.81 \cdot 10^{-10}$	$2.32 \cdot 10^{-9}$	385.6
	$2.00 \cdot 10^{4}$	$6.55 \cdot 10^{-9}$	$2.25 \cdot 10^{-10}$	$8.52 \cdot 10^{-10}$	215.1
	$3.16 \cdot 10^{4}$	$2.05 \cdot 10^{-9}$	$8.78 \cdot 10^{-11}$	$2.95 \cdot 10^{-10}$	107.5
	$5.01 \cdot 10^{4}$	$6.56 \cdot 10^{-10}$	$4.04 \cdot 10^{-11}$	$1.13 \cdot 10^{-10}$	54.4
	$7.94 \cdot 10^{4}$	$2.02 \cdot 10^{-10}$	$1.58 \cdot 10^{-11}$	$4.31 \cdot 10^{-11}$	26.0
	$1.26 \cdot 10^{5}$	$6.02 \cdot 10^{-11}$	$6.70 \cdot 10^{-12}$	$1.74 \cdot 10^{-11}$	12.3

	$7.94 \cdot 10^{3}$	$1.05 \cdot 10^{-6}$	$5.14 \cdot 10^{-9}$	$1.17 \cdot 10^{-7}$	7882.5
	$1.26 \cdot 10^{4}$	$3.45 \cdot 10^{-7}$	$2.14 \cdot 10^{-9}$	$3.88 \cdot 10^{-8}$	4455.5
All	$2.00 \cdot 10^{4}$	$1.14 \cdot 10^{-7}$	$9.58 \cdot 10^{-10}$	$1.29 \cdot 10^{-8}$	2356.2
nuclei	$3.16 \cdot 10^{4}$	$3.54 \cdot 10^{-8}$	$3.69 \cdot 10^{-10}$	$4.10 \cdot 10^{-9}$	1267.9
	$5.01 \cdot 10^{4}$	$1.11 \cdot 10^{-8}$	$1.59 \cdot 10^{-10}$	$1.32 \cdot 10^{-9}$	633.3
	$7.94 \cdot 10^{4}$	$3.32 \cdot 10^{-9}$	$5.91 \cdot 10^{-11}$	$4.28 \cdot 10^{-10}$	302.0
	$1.26 \cdot 10^{5}$	$9.94 \cdot 10^{-10}$	$2.55 \cdot 10^{-11}$	$1.48 \cdot 10^{-10}$	145.1
	$2.00 \cdot 10^{5}$	$2.90 \cdot 10^{-10}$	$9.38 \cdot 10^{-12}$	$5.09 \cdot 10^{-11}$	69.4
	$3.16 \cdot 10^{5}$	$8.17 \cdot 10^{-11}$	$3.92 \cdot 10^{-12}$	$1.83 \cdot 10^{-11}$	31.1
	$5.01 \cdot 10^{5}$	$2.29 \cdot 10^{-11}$	$1.49 \cdot 10^{-12}$	$6.87 \cdot 10^{-12}$	14.4
	$7.94 \cdot 10^{5}$	$6.07 \cdot 10^{-12}$	$6.12 \cdot 10^{-13}$	$2.75 \cdot 10^{-12}$	6.0

The KLEM and calorimeter data are almost independent because energy measurements are based on different detectors and different methods. Moreover the geometric factor for the calorimeter is significantly less than for the KLEM detector. Only about a quarter of events registered by the KLEM detector is registered also by IC. Therefore errors for the KLEM technique are reduced in comparison to the IC. The NUCLEON spectra are compared with results of different experiments (ATIC (Ahn et al., 2006, Panov et al., 2006), CREAM (Yoon et al., 2011, Ahn et al., 2009), TRACER (Obermeier et al., 2011), AMS02 (Aguilar et al., 2015a, 2015b), SOKOL (Ivanenko et al., 1993)).

The all particles spectra are presented in fig.19 in comparison with space and EAS experiments.

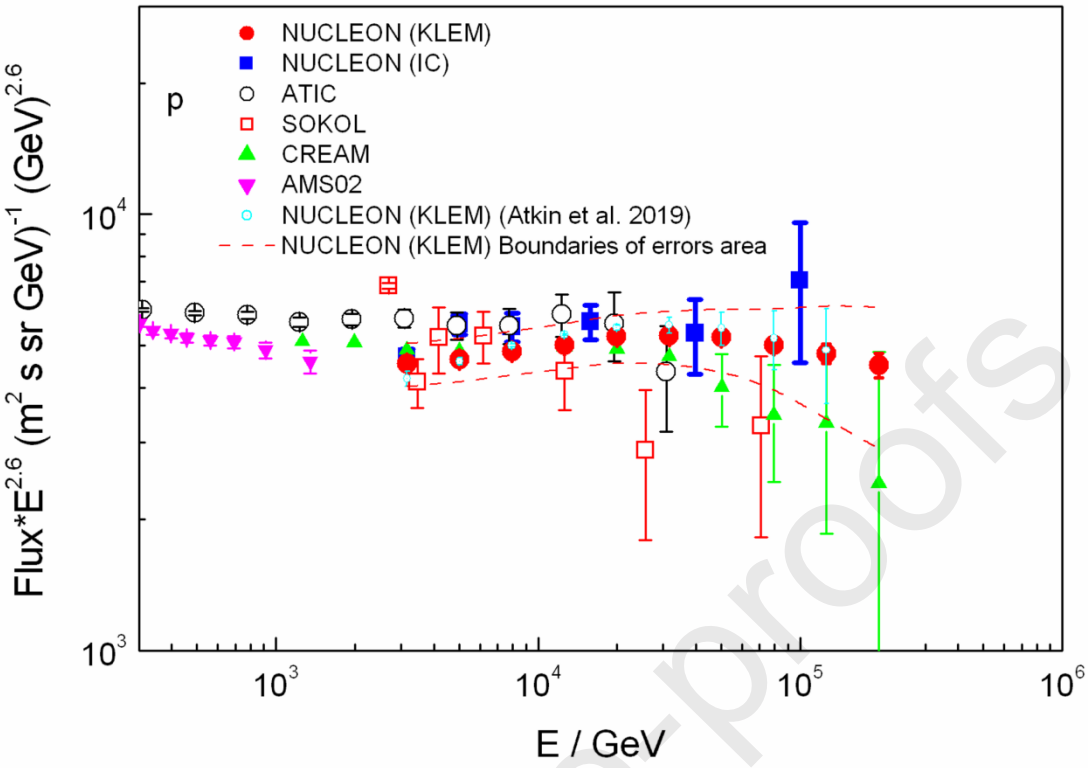

Figure 11. Proton spectrum.

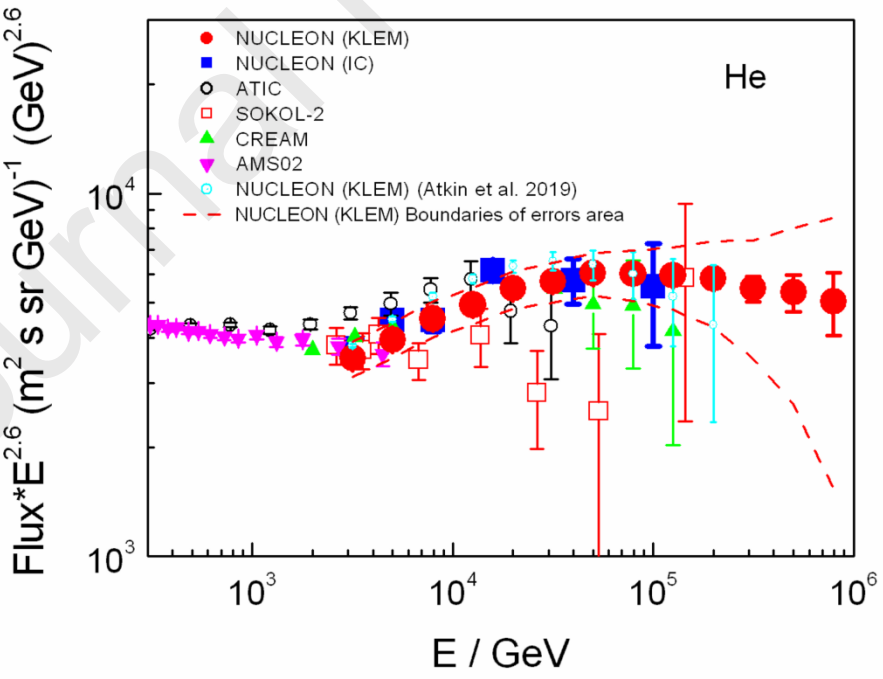

Figure 12. Helium spectrum.

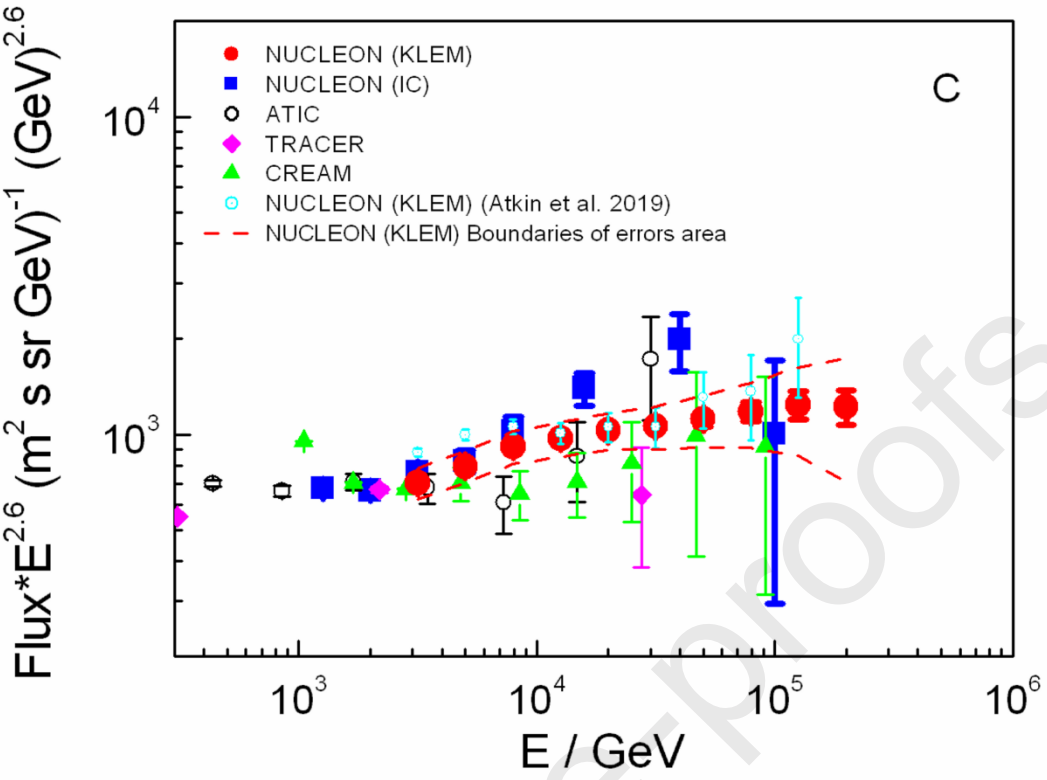

Figure 13. Carbon spectrum.

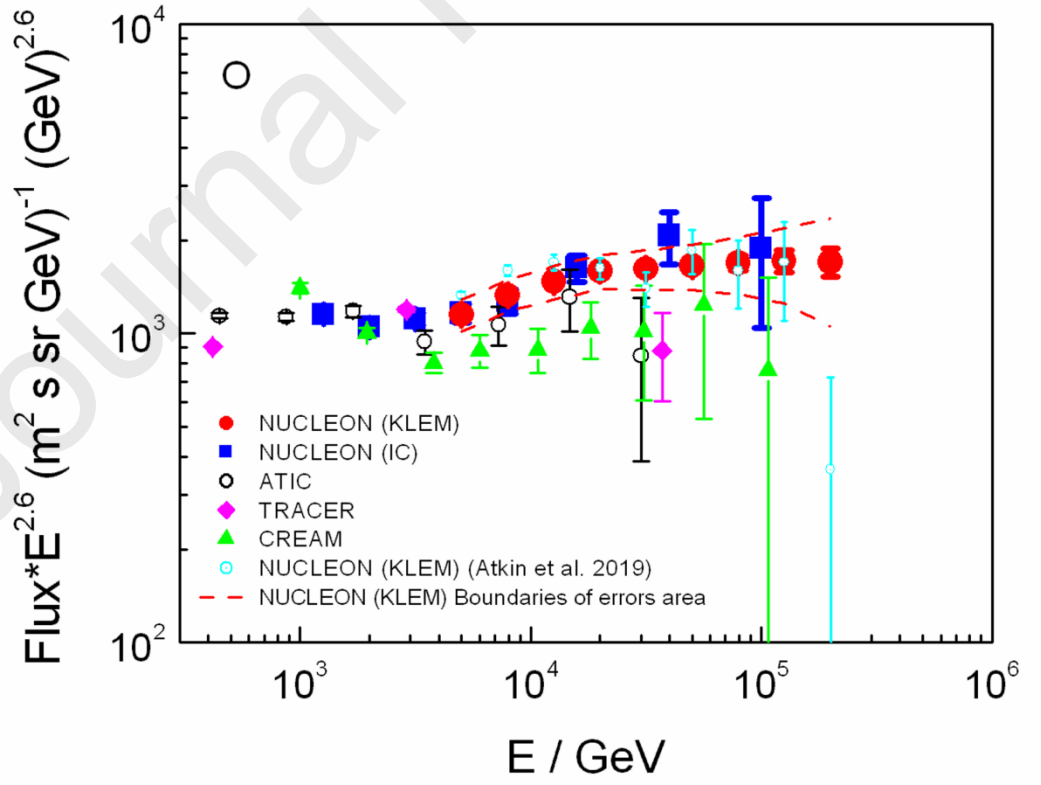

Figure 14. Oxygen spectrum.

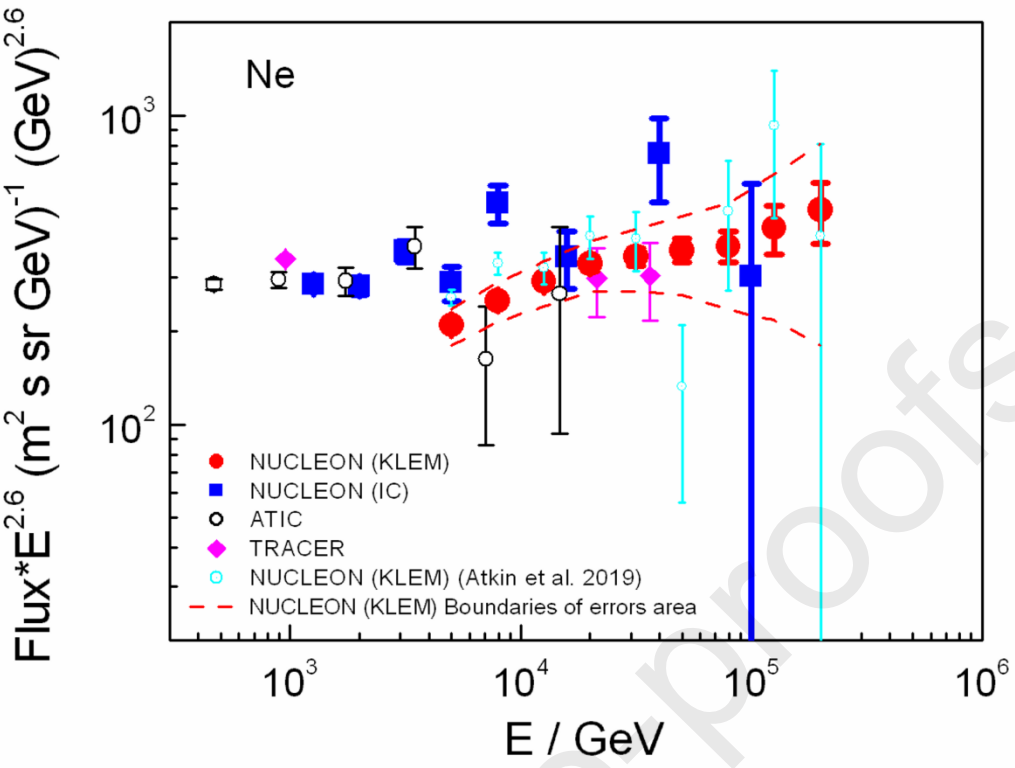

Figure 15. Neon spectrum.

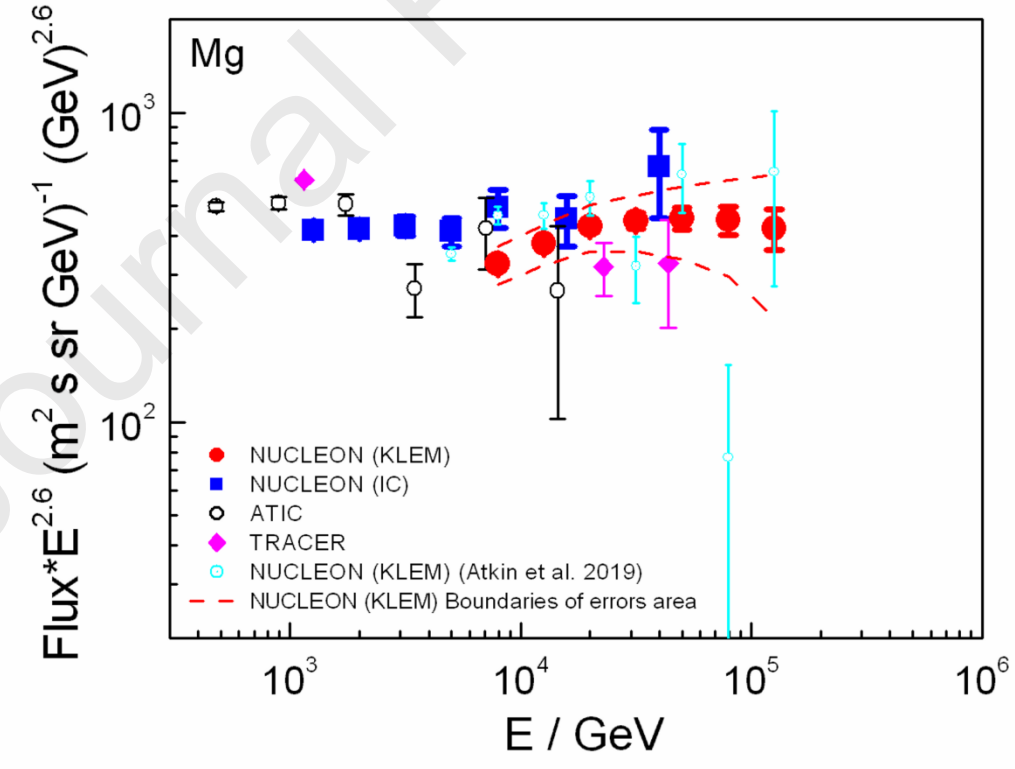

Figure 16. Magnesium spectrum.

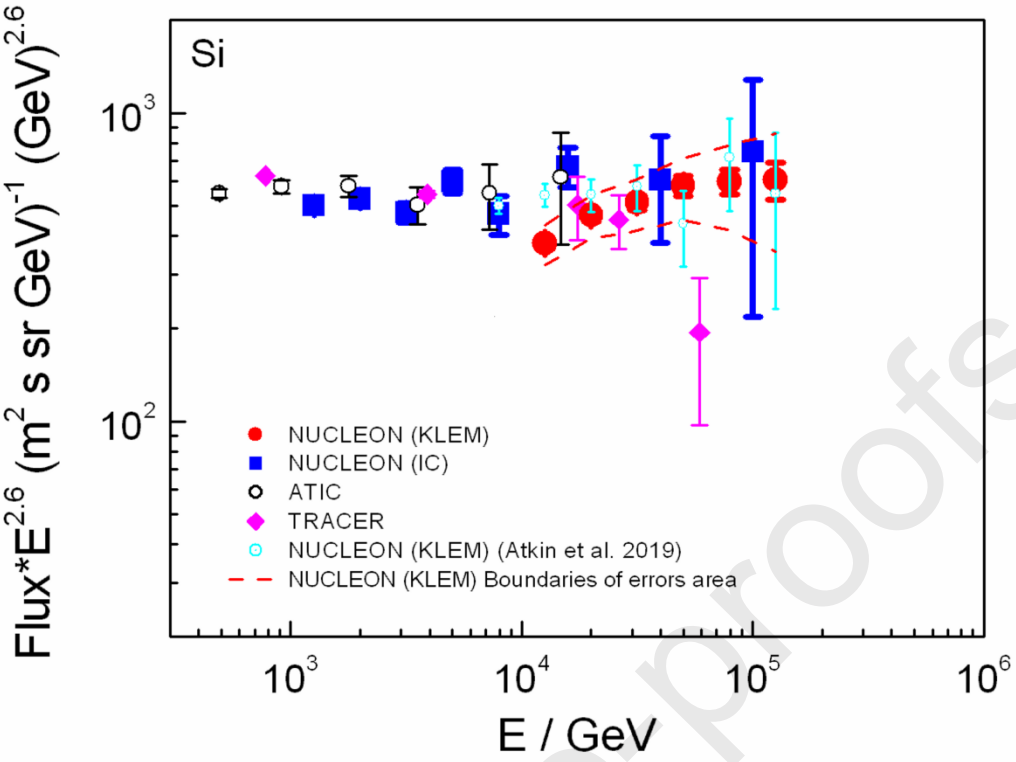

Figure 17. Silicon spectrum.

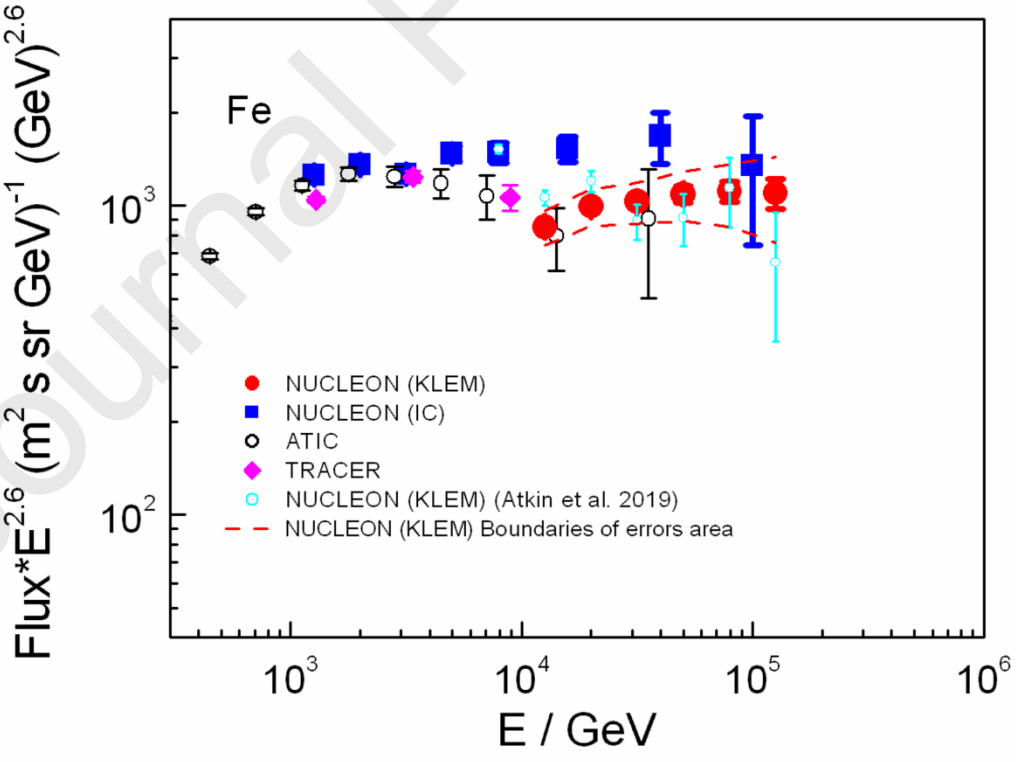

Figure 18. Iron spectrum.

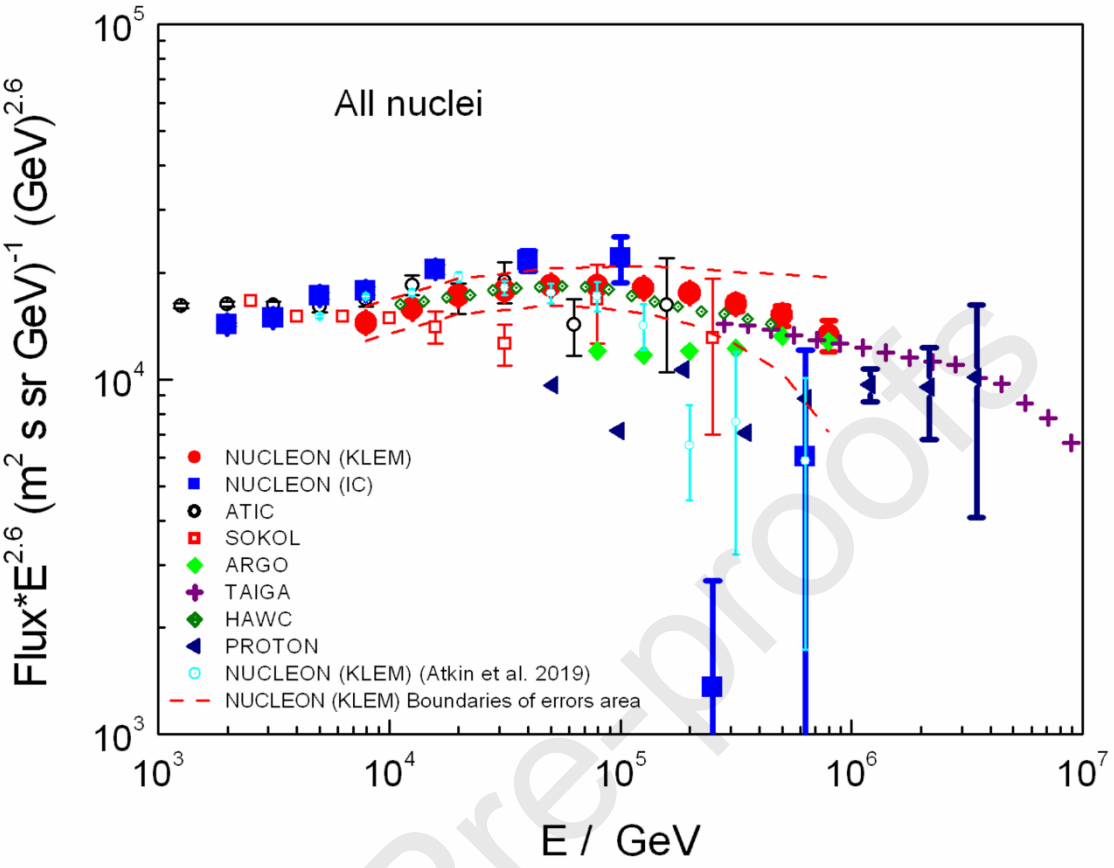

Figure 19. All particles spectrum.

We can see some spectral peculiarities energies ~10 TeV. It can be interpreted by general dependence on magnetic rigidity (Atkin et al., 2018).

The results of the NUCLEON experiment showed existence of an universal break near the magnetic rigidity 10 TV in all abundant nuclear components of cosmic rays (Atkin et al., 2018). Fig.20 shows the spectra of protons and helium nuclei obtained above by deconvolution procedure in terms of magnetic rigidities along with the original rigidity spectra measured in (Atkin et al., 2018). It was reported in (Atkin et al., 2018) that the joint rigidity spectrum of all heavy nuclei from carbon to iron also shows a break near 10 TV.

Now we apply deconvolution and evaluate systematic errors. The boundaries of errors area are presented in fig.20. Even taking into account the calculated values of systematic errors the spectra can not be described by an unified power

law in the all rigidity range. Systematic errors in the reconstruction of energy can only shift the spectra left or right and uniformly change the absolute fluxes at all energies. Some uncertainties in the apparatus acceptance may uniformly change a bit the slope of the spectra. But systematic errors can not drastically change the shape of the spectra.

This break will be studied in detail in forthcoming works.

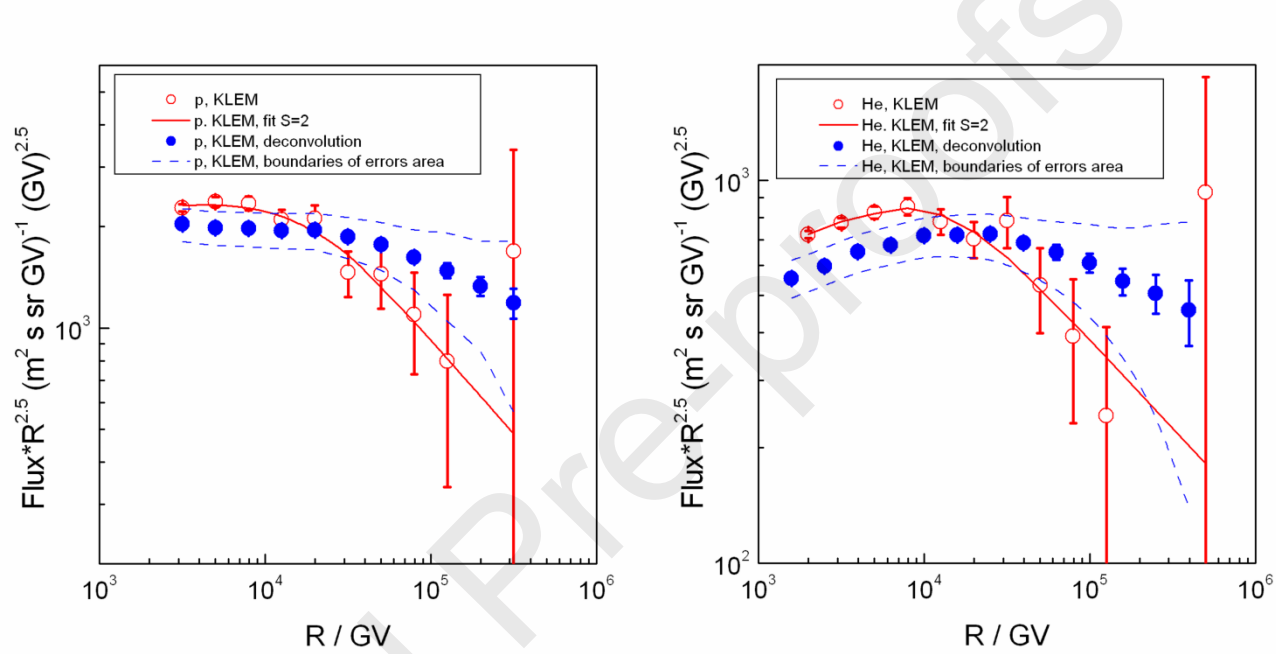

Figure 20. Magnetic rigidity spectra of protons and helium nuclei obtained by deconvolution procedure in this paper along with the original rigidity spectra measured in (Atkin et al., 2018). Red line is an approximation of the measured spectra by double power law function with the link smooth parameter $S = 2$ (see details in (Atkin et al., 2018).

8. Discussion and conclusions

The obtained energy spectra show good consensus on two different techniques of energy measurements. Thus, operability of a new KLEM technique in the wide energy range is confirmed.

Comparison of the energy spectra obtained by the NUCLEON experiment, and the results of other experiments, show good similarity to the energy range studied previously. At the same time, the NUCLEON data stretch to the area of

energies higher than 100 TeV/particle for abundant nuclei, where there are no other experiments or their statistical material is too small.

Remarkable pecularities of spectra are observed. The spectra can not be described by an unified power law in the all rgidity range. Systematic errors can not drastically change the shape of spectra. The measured shape of spectra can possibly be explained by the presence of a few local sources of cosmic rays (Keum and Salati, 2016) or different types of sources (Zatsepin and Sokolskaya, 2006).

Now we work on a more detailed validation of Monte-Carlo simulation to improve the energy spectra reconstrution.

Acknowledgments

We acknowledge support from the Russian Space Agency (RosCosmos), Russian Academy of Sciences (RAS), JSC SRC Progress.

References

Adams, J., Bashindzhagyan, G., Chilingarian, A., Drury, L., Egorov, N., Golubkov, S., Korotkova, N., Panasyuk, M., Podorozhnyi, D., Procureur, J., Roganova, T., Saavedra, O., Sidorov, A., Simon, M., Sveshnikova, L., Turundaevsky, A., Yashin. I., 2000. Particle energy determination device for the international space station using a new approach to cosmic ray spectral measurements (TUS-M mission). AIP Conference Proceedings 504, 175-180. CP504, Space Tecnology and Applications International Forum-2000, edited by M.S.El-Genk, AIP Publishing Center, Melville, NY, USA, DOI: 10.1063/1.1302477

Adams, J., Bashindzhagyan, G., Bashindzhagyan, P., Chilingarian, A., Drury, L., Egorov, N., Golubkov, S., Korotkova, N., Menn, W., Panasyuk, M., Podorozhnyi, D., Procureur, J., Roganova, T., Saavedra, O., Sidorov, A., Simon, M., Sveshnikova, L., Thompson, A., Turundaevsky, A., Yashin. I., 2001. An instrument to measure elemental energy spectra of cosmic-ray nuclei up to 10^{16} eV. Advances in Space Research 27, 829-833. DOI: 10.1016/S0273-1177(01)00127-2

Aguilar, M., Aisa, D., Alpat, B. et al (AMS collaboration), 2015. Precision Measurement of the Helium Flux in Primary Cosmic Rays of Rigidities 1.9 GV to 3 TV with the Alpha Magnetic Spectrometer on the International Space Station. Phys. Rev. Lett. 115, 211101. DOI: 10.1103/PhysRevLett.115.211101.

Aguilar, M., Aisa, D., Alpat, B. et al (AMS collaboration), 2015. Precision Measurement of the Proton Flux in Primary Cosmic Rays from Rigidity 1 GV to 1.8 TV with the Alpha Magnetic Spectrometer on the International Space Station. Phys. Rev. Lett. 114, 171103. DOI: 10.1103/PhysRevLett.114.171103.

Aguilar, M., Ali Cavasonza, L., Alpat, B. et al. (AMS collaboration), 2017. Observation of the Identical Rigidity Dependence of He, C, and O Cosmic Rays at High Rigidities by the Alpha Magnetic Spectrometer on the International Space Station. Phys. Rev. Lett. 119, 251101. DOI: 10.1103/PhysRevLett.119.251101

Aguilar, M., Ali Cavasonza, L., Ambrosi, G. et al. (AMS collaboration), 2018. Observation of New Properties of Secondary Cosmic Rays Lithium, Beryllium, and Boron by the Alpha Magnetic Spectrometer on the International Space Station. Phys. Rev. Lett. 120, 021101. DOI: 10.1103/PhysRevLett.120.021101

Aguilar, M., Ali Cavasonza, L., Alpat, B. et al. (AMS collaboration), 2018. Precision Measurement of Cosmic-Ray Nitrogen and its Primary and Secondary Components with the Alpha Magnetic Spectrometer on the International Space Station. Phys. Rev. Lett. 121, 051103. DOI: 10.1103/PhysRevLett.121.051103

Ahn, H.S. , Seo, E.S., Ganel, O., Kim, K.C. , Sina, R., Wang, J.Z., Wu, J., Adams, J.H., Christl, M., Bashindzhagyan, G., Batkov, K.E., Kouznetsov, E., Panasyuk, M., Panov, A., Sokolskaya, N.V., Zatsepin, V., Chang, J., Schmidt, W.K.H., Fazely, A.R., Gunasingha, R.M., 2006. The energy spectra of protons and helium measured with the ATIC experiment. Advances in Space Research 37, 1950-1954. DOI: 10.1016/j.asr.2005.09.031 .

Ahn, H.S., Allison, P., Bagliesi, M.G., Barbier, L., Beatty, J.J., Bigongiari, G., Brandt, T.J., Childers, J.T., Conklin, N.B., Coutu, S., DuVernois, M.A., Ganel, O., Han, J.H., Jeon, J.A., Kim, K.C., Lee, M.H., Maestro, P., Malinine, A.,

Marrocchesi, P.S., Minnick, S., Mognet, S.I., Nam, S.W., Nutter, S., Park, I.H., Park, N.H., Seo, E.S., Sina, R., Walpole, P., Wu, J., Yang, J., Yoon, Y.S., Zei, R., Zinn, S.Y., 2009. Energy spectra of cosmic-ray nuclei at high energies. The Astrophysical Journal, 707, 593-603. DOI: 10.1088/0004-637X/707/1/593

Atkin, E., Bulatov, V., Dorokhov, V., Gorbunov, N., Filippov, S., Grebenyuk, V., Karmanov, D., Kovalev, I., Kudryashov, I., Merkin, M., Pakhomov, A., Podorozhny, D., Polkov, D., Porokhovoy, S., Shumikhin, V., Sveshnikova, L., Tkachenko, A., Tkachev, L., Turundaevskiy, A., Vasiliev, O., Voronin, A., 2015. The NUCLEON space experiment for direct high energy cosmic rays investigation in TeV–PeV energy range. Nuclear Instruments and Methods in Physics Research, Section A: Accelerators, Spectrometers, Detectors and Associated Equipment, 770, 189-196. DOI:10.1016/j.nima.2014.09.079

Atkin, E., Bulatov, V., Dorokhov, V., Gorbunov, N., Filippov, S., Grebenyuk, V., Karmanov, D., Kovalev, I., Kudryashov, I., Kurganov, A., Merkin, M., Pakhomov, A., Podorozhny, D., Polkov, D., Porokhovoy, S., Shumikhin, V., Sveshnikova, L., Tkachenko, A., Tkachev, L., Torochkov, M., Turundaevskiy, A., Vasiliev, O., Voronin, A., 2015. The NUCLEON space experiment. EPJ Web of Conferences 105, 01002–p1–01002–p4. DOI**:**10.1051/epjconf/201510501002

Atkin, E., Voronin, A., Karmanov, D., Kudryashov, I., Podorozhniy, D., Shumikhin, V., 2015. The read-out asic for the space nucleon project. Journal of Instrumentation, 10:C04005. DOI: 10.1088/1748-0221/10/04/C04005

Atkin, E., Bulatov, V., Dorokhov, V., Gorbunov, N., Filippov, S., Grebenyuk, V., Karmanov, D., Kovalev, I., Kudryashov, I., Kurganov, A., Merkin, M., Panov, A., Podorozhny, D., Polkov, D., Porokhovoy, S., Shumikhin, V., Sveshnikova, L., Tkachenko, A., Tkachev, L., Turundaevskiy, A., Vasiliev, O., Voronin, A., 2017.

First results of the cosmic ray nucleon experiment. Journal of Cosmology and Astroparticle Physics, 2017(7):20.

Atkin, E., Bulatov, V., Dorokhov, V., Filippov, S., Gorbunov, N., Grebenyuk, V., Karmanov, D., Kovalev, I., Kudryashov, I., Kurganov, A., Merkin, M., Panov, A., Podorozhny, D., Polkov, D., Porokhovoy, S., Shumikhin, V., Sveshnikova, L., Tkachenko, A., Tkachev, L., Turundaevskiy, A., Vasiliev, O., Voronin, A., 2017. The NUCLEON experiment. Results of the first year of data acquisition. Astroparticle Physics 90, 64-74. DOI: 10.1016/j.astropartphys.2017.02.006

Atkin, E., Bulatov, V., Dorokhov, V., Gorbunov, N., Filippov, S., Grebenyuk, V., Karmanov, D., Kovalev, I., Kudryashov, I., Merkin, M., Pakhomov, A., Panov, A., Podorozhny, D., Polkov, D., Porokhovoy, S., Shumikhin, V., Sveshnikova, L., Tkachenko, A., Tkachev, L., Torochkov, M., Turundaevskiy, A., Vasiliev, O., Voronin, A., 2017. The NUCLEON Space Experiment - Preliminary Results. Proceedings of Science. Frontier Research in Astrophysics – II. 23-28 May 2016 Mondello (Palermo), Italy. PoS(FRAPWS2016) 269, 090. DOI:10.22323/1.269.0090

Atkin, E., Bulatov, V., Dorokhov, V., Filippov, S., Gorbunov, N., Grebenyuk, V., Karmanov, D., Kovalev, I., Kudryashov, I., Kurganov, A., Merkin, M., Panov, A., Podorozhny, D., Polkov, D., Porokhovoy, S., Shumikhin, V., Sveshnikova, L., Tkachenko, A., Tkachev, L., Turundaevskiy, A., Vasiliev, O., Voronin, A., 2018. New universal cosmic-ray knee near a magnetic rigidity of 10TV with the NUCLEON space observatory. JETP Letters 108, 5-12. DOI: 10.1134/S0021364018130015

Atkin, E., Bulatov, V., Dorokhov, V., Gorbunov, N., Filippov, S., Grebenyuk, V., Karmanov, D., Kovalev, I., Kudryashov, I., Kurganov, A., Merkin, M., Panov, A.,

Podorozhny, D., Polkov, D., Porokhovoy, S., Shumikhin, V., Sveshnikova, L., Tkachenko, A., Tkachev, L., Turundaevskiy, A., Vasiliev, O., Voronin, A., 2019. Energy spectra of cosmic ray protons and nuclei measured by the NUCLEON experiment by means of the new method. Astronomy Reports 63, 66-78. DOI: 10.1134/S1063772919010013

Bashindzhagyan, G.L., Voronin, A.G., Golubkov, S.A., Grebenyuk, V.M., Egorov, N.N., Kalinin, A.M., Karmanov, D.E., Kon'kov, K.A., Korotkova, N.A., Kozlov, Y.F., Krumshtein, Z.V., Merkin, M.M., Panasyuk, M.I., Pakhomov, A.Y., Podorozhnyi, D.M., Postnikov, E.B., Roganova, T.M., Sadovskii, A.B., Sveshnikova, L.G., Sidorov, A.I., Tkachev, L.G., Turundaevskii, A.N., 2005. A new method for determining particle energy in the range 10^{11}-10^{15} eV and results from a beam test at 180 GeV/c. Instruments and Experimental Techniques 48, 32-36. DOI: 10.1007/s10786-005-0004-3

Batkov, K., Bigongiari, G., Maestro, P., Marrocchesi, P.S., Kim, M.Y., Zei, R., 2011. Direct measurements of cosmic-ray energy: the kinematical method revisited. Astroparticle Physics 35, 50-61. DOI:10.1016/j.astropartphys.2011.06.002

Brogi, P., Marrocchesi, P., Maestro, P., Mori N., 2016. CALET measurements with cosmic nuclei: expected performances of tracking and charge identification. Proc. 34th ICRC. Hague, Netherlands. PoS ICRC2015 , 595.

Brun, R., 1993. GEANT User's Guide. CERN DD/EE/83/1. Geneva, 1983.

Bulatov, V.L., Vlasov, A.V., Gorbunov, N.V., Grebenyuk, V.M., Karmanov, D.E., Pakhomov, A.Yu., Podorozhnyi, D.M., Polkov, D.A., Tkachev, L.G., Tkachenko, A.V., Tarabrin, S.P., Turundaevskii, Filippov, S.B., 2010. Testing the engineering

sample of the NUCLEON setup on a pion beam. Instruments and Experimental Techniques. 53, 29-35. DOI: 10.1134/S0020441210010033 .

Castagnoli, C., Gortini, G., Franzinetti, C., Manfredini, A., Moreno, D., 1953. An investigation on jets. Nuovo Cimento 10, 1539-1558.
DOI: 10.1007/BF02854918

Ivanenko, I.P., Shestoperov, V.Ya., Chikova, L.O., Fateeva, I.M., Khein, L.A., Podorozhnyi, D.M., Rapoport, I.D., Samsonov, G.A., Sobinyakov, V.A., Turundaevskii, A.N., Yashin, I.V., 1993. Energy spectra of cosmic rays above 2 TeV as measured by the SOKOL apparatus. Proc. 23 ICRC 2, 17-19. Calgary. Canada.

Kalmykov, N.N., Ostapchenko, S.S., Pavlov, A.I., 1997. Quark-gluon-string model and EAS simulation problems at ultra-high energies. Nucl. Phys. B (Proc. Suppl.) 52, 17-28. DOI: 10.1016/S0920-5632(96)00846-8

Keum, Y., Salati, P., 2016. The TeV-scale cosmic ray proton and helium spectra: Contributions from the local sources. Pramana – Journal of Physics 86, 369. DOI:10.1007/s12043-015-1157-7

Korotkova, N.A., Podorozhnyi, D.M., Postnikov, E.B., Roganova, T.M., Sveshnikova, L.G., Turundaevsky, A.N., 2002. New method for determining energies of cosmic-ray nuclei. Physics of Atomic Nuclei 65, 852-860.
DOI: 10.1134/1.1481478

Obermeier, A., Ave, M., Boyle, P., Hoppner, Ch., Horandel, J., Muller, D., 2011. Energy spectra oprimary and secondary cosmic-ray nuclei measured with TRACER. The Astrophysical Journal, 742,14. DOI: 10.1088/0004-637X/742/1/14

Panov, A.D., Adams, J.H. Jr, Ahn, H.S., Bashindzhagyan, G.L., Batkov, K.E., Chang, J., Christl, M., Fazely, A.R., Ganel, O., Gunasingha, R.M., Guzik, T.G., Isbert, J., Kim, K.C. , Kouznetsov, E.N., Panasyuk, M.I., Schmidt, W.K.H., Seo, E.S., Sokolskaya, N.V., Wefel, J.P., Wu, J., Zatsepin V.I., 2006. The energy spectra of heavy nuclei measured by the ATIC experiment. Advances in Space Research 37, 1944-1949. DOI: 10.1016/j.asr.2005.07.040 .

Podorozhnyi, D.M., Postnikov, E.B., Sveshnikova, L.G., Turundaevsky, A.N., 2005. Application of a multivariate statistical technique to interpreting data from multichannel equipment for the example of the KLEM spectrometer. Physics of Atomic Nuclei 68, 50-59. DOI: 10.1134/1.1858557

Podorozhnyi, D.M., Bulatov, V.L., Baranova, N.V., Vlasov, A.V., Voronin, A.G., Egorov, N.N., Golubkov, S.A., Grebenyuk, V.M., Karmanov, D.E., Korolev, M.G., Korotkova, N.A., Krumshtein, Z.V., Lyannoy, E.G., Merkin, M.M., Pavlov, A.Yu., Pakhomov, A.Yu., Romanov, A.V., Sadovskii, A.B., Sveshnikova, L.G., Tkachev, L.G., Tkachenko, A.V., Turundaevskiy, A.N., 2007. The NUCLEON experiment: The current status. Bulletin of the Russian Academy of Sciences: Physics 71, 500-502. DOI: 10.3103/S1062873807040181

Postnikov, E.B., Bashindzhagyan, G.L., Korotkova, N.A., Podorozhny, D.M., Roganova, T.M., Sveshnikova, L.G., Turundaevsky A.N., 2002. Method of energy determination for KLEM spectrometer in NUCLEON project by statistical estimation of random vectors. IZVESTIYA AKADEMII NAUK SERIYA FIZICHESKAYA 66, 1634-1637 (Bulletin of the Russian Academy of Sciences: Physics 66, 1806-1809).

Seo, E.S., Anderson, T., Angelaszek, D., Baek, S.J., Baylon, J., Buenerd, M., Copley, M., Coutu, S., Derome, L., Fields, B., Gupta, M., Han, J.H., Howley, I.J., Huh, H.G., Hwang, Y.S., Hyun, H.J., Jeong, I.S., Kah, D.H., Kang, K.H., Kim,

D.Y., Kim, H.J., Kim, K.C., Kim, M.H., Kwashnak, K., Lee, J., Lee, M.H., Link, J.T., Lutz, L., Malinin, A., Menchaca-Rocha, A., Mitchell, J.W., Nutter, S., Ofoha, O., Park, H., Park, I.H., Park, J.M., Patterson, P., Smith, J.R., Wu, J., Yoon Y.S., 2014. Cosmic Ray Energetics And Mass for the International Space Station (ISS-CREAM). Advances in Space Research 53, 1451-1455.
DOI: 10.1016/j.asr.2014.01.013

Vasiliev, O.A., Karmanov, D.E., Kovalyov, I.M., Kudryashov, I.A., Lobanov, A.A., Podorozhnyi, D.M., Tkachev, L.G., Tkachenko, A.V., Turundaevskiy, A.N., Shigaev V.N., 2014. Separation of the electron component by the shower shape in an ionization calorimeter for the nucleon experiment. Physics of Atomic Nuclei, 77, 587-594. DOI: 10.1134/S1063778814050123 .

Voronin, A.G., Grebenyuk, V.M., Karmanov, D.E., Korotkova, N.A., Krumshtein, Z.V., Merkin, M.M., Pakhomov, A.Yu., Podorozhnyi, D.M., Sadovskii, A.B., Sveshnikova, L.G., Tkachev, L.G., Turundaevsky, A.N., 2007. Testing a prototype of the charge-measuring system for the NUCLEON setup. Instruments and Experimental Techniques. 50, 187-195. DOI: 10.1134/S0020441207020030

Voronin, A.G., Grebenyuk, V.M., Karmanov, D.E., Korotkova, N.A., Krumshtein, Z.V., Merkin, M.M., Pakhomov, A.Yu., Podorozhnyi, D.M., Sadovskii, A.B., Sveshnikova, L.G., Tkachev, L.G., Turundaevsky, A.N., 2007. Testing a prototype of the NUCLEON setup on the pion beam. Instruments and Experimental Techniques. 50, 176-186. DOI: 10.1134/S0020441207020029.

Wu, X., Ambrosi, G., Asfandiyarov, R., Azzarello, P., Bernardini, P., Bertucci, B., Bolognini, A., Cadoux, F., Caprai, M., De Mitri, I., Dong, Y., Duranti, M., Fan, R., Fusco, P., Gallo, V., Gargano, F., Guo, D., Husi, C., Ionica, M., Ke, G., La Marra, D., Loparco, F., Marsella, G., Mazziotta, M.N., Nardinocchi, A., Nicola, L., Pelleriti, G., Peng, W., Postolache, V., Pohl, M., Qiao, R., Surdo, A., Tykhonov,

A., Vitillo, S., Wang, H., Weber, M., Wu, D., Zhang, F., 2016. The Silicon-Tungsten Tracker of the DAMPE Mission. Proc. 34th ICRC. Hague, Netherlands. PoS ICRC2015 , 1192.

Yoon, Y.S., Ahn, H.S., Allison, P.S., Bagliesi, M.G., Beatty, J.J., Bigongiari, G., Boyle, P.J., Childers, J.T., Conklin, N.B., Coutu, S., DuVernois, M.A., Ganel, O., Han, J.H., Jeon, J.A., Kim, K.C., Lee, M.H., Lutz, L., Maestro, P., Malinin, A., Marrocchesi, P.S., Minnick, S.A., Mognet, S.I., Nam, S., Nutter, S., Park, I.H., Park, N.H., Seo, E.S., Sina, R., Swordy, S., Wakely, S.P., Wu, J., Yang, J., Zei, R., Zinn, S.Y., 2011. Cosmic-ray proton and helium spectra from the first CREAM flight. The Astrophysical Journal, 728, 122. DOI: 10.1088/0004-637X/728/2/122

Yoon, Y.S., Anderson, T., Barrau, A., Conklin, N.B., Coutu, S., Derome, L., Han, J.H., Jeon, J.A., Kim, K.C., Kim, M.H., Lee, H.Y., Lee, J., Lee, M. H., Lee, S. E., Link, J.T., Menchaca-Rocha, A., Mitchell, J.W., Mognet, S.I., Nutter, S., Park, I.H., Picot-Clemente, N., Putze, A., Seo, E.S., Smith, J., Wu, J., 2017. Proton and Helium Spectra from the CREAM-III Flight. The Astrophysical Journal, 839, 5. DOI: 10.3847/1538-4357/aa68e4

Zatsepin, V.I., Sokolskaya, N.V., 2006. Three component model of cosmic ray spectra from 10 GeV to 100 PeV. Astronomy and Astrophysics 458, 1–5.

Table 1. Energy reconstruction parameters

Projectile nucleus	a_2 GeV	b
p	1651±82	1.357±0.009
He	2556±125	1.274±0.008
C	3514±199	1.180±0.009
S	4163±230	1.141±0.008
Fe	4362±195	1.119±0.007

Table 2. Deconvoluted energy spectra obtained by the NUCLEON experiment

Particle	Energy, GeV	Flux (m2 sr s GeV)$^{-1}$	Statistical error	Systematic error	ΔN_{cor}
Protons	$3.16\cdot10^{3}$	$3.62\cdot10^{-6}$	$1.99\cdot10^{-8}$	$4.07\cdot10^{-7}$	4920.9
	$5.01\cdot10^{3}$	$1.11\cdot10^{-6}$	$8.16\cdot10^{-9}$	$1.26\cdot10^{-7}$	2866.0
	$7.94\cdot10^{3}$	$3.51\cdot10^{-7}$	$3.55\cdot10^{-9}$	$4.01\cdot10^{-8}$	1432.7
	$1.26\cdot10^{4}$	$1.09\cdot10^{-7}$	$1.40\cdot10^{-9}$	$1.29\cdot10^{-8}$	822.5
	$2.00\cdot10^{4}$	$3.46\cdot10^{-8}$	$6.21\cdot10^{-10}$	$4.25\cdot10^{-9}$	412.9
	$3.16\cdot10^{4}$	$1.05\cdot10^{-8}$	$2.23\cdot10^{-10}$	$1.44\cdot10^{-9}$	217.1
	$5.01\cdot10^{4}$	$3.15\cdot10^{-9}$	$9.10\cdot10^{-11}$	$5.00\cdot10^{-10}$	103.5
	$7.94\cdot10^{4}$	$9.13\cdot10^{-10}$	$3.22\cdot10^{-11}$	$1.82\cdot10^{-10}$	52.3
	$1.26\cdot10^{5}$	$2.63\cdot10^{-10}$	$1.35\cdot10^{-11}$	$7.58\cdot10^{-11}$	24.1
	$2.00\cdot10^{5}$	$7.48\cdot10^{-11}$	$4.78\cdot10^{-12}$	$2.62\cdot10^{-11}$	11.2
He	$3.16\cdot10^{3}$	$2.79\cdot10^{-6}$	$1.43\cdot10^{-8}$	$3.12\cdot10^{-7}$	7062.6
	$5.01\cdot10^{3}$	$9.49\cdot10^{-7}$	$6.24\cdot10^{-9}$	$1.06\cdot10^{-7}$	4114.6
	$7.94\cdot10^{3}$	$3.28\cdot10^{-7}$	$2.83\cdot10^{-9}$	$3.70\cdot10^{-8}$	2255.3
	$1.26\cdot10^{4}$	$1.08\cdot10^{-7}$	$1.14\cdot10^{-9}$	$1.23\cdot10^{-8}$	1235.1
	$2.00\cdot10^{4}$	$3.61\cdot10^{-8}$	$5.22\cdot10^{-10}$	$4.22\cdot10^{-9}$	654.7
	$3.16\cdot10^{4}$	$1.14\cdot10^{-8}$	$2.11\cdot10^{-10}$	$1.41\cdot10^{-9}$	384.4
	$5.01\cdot10^{4}$	$3.64\cdot10^{-9}$	$9.22\cdot10^{-11}$	$4.80\cdot10^{-10}$	194.0
	$7.94\cdot10^{4}$	$1.09\cdot10^{-9}$	$3.40\cdot10^{-11}$	$1.70\cdot10^{-10}$	92.1
	$1.26\cdot10^{5}$	$3.26\cdot10^{-10}$	$1.43\cdot10^{-11}$	$6.21\cdot10^{-11}$	43.9
	$2.00\cdot10^{5}$	$9.68\cdot10^{-11}$	$5.39\cdot10^{-12}$	$2.52\cdot10^{-11}$	21.6
	$3.16\cdot10^{5}$	$2.74\cdot10^{-11}$	$2.19\cdot10^{-12}$	$9.57\cdot10^{-12}$	9.8
	$5.01\cdot10^{5}$	$8.07\cdot10^{-12}$	$9.32\cdot10^{-13}$	$4.01\cdot10^{-12}$	4.8
	$7.94\cdot10^{5}$	$2.31\cdot10^{-12}$	$4.51\cdot10^{-13}$	$1.54\cdot10^{-12}$	2.2
C	$3.16\cdot10^{3}$	$5.59\cdot10^{-7}$	$5.56\cdot10^{-9}$	$6.28\cdot10^{-8}$	2248.7
	$5.01\cdot10^{3}$	$1.91\cdot10^{-7}$	$2.40\cdot10^{-9}$	$2.18\cdot10^{-8}$	1298.1
	$7.94\cdot10^{3}$	$6.63\cdot10^{-8}$	$1.09\cdot10^{-9}$	$7.75\cdot10^{-9}$	715.6
	$1.26\cdot10^{4}$	$2.13\cdot10^{-8}$	$4.59\cdot10^{-10}$	$2.58\cdot10^{-9}$	379.4
	$2.00\cdot10^{4}$	$6.80\cdot10^{-9}$	$1.92\cdot10^{-10}$	$8.85\cdot10^{-10}$	192.9
	$3.16\cdot10^{4}$	$2.12\cdot10^{-9}$	$7.58\cdot10^{-11}$	$3.13\cdot10^{-10}$	100.2
	$5.01\cdot10^{4}$	$6.74\cdot10^{-10}$	$3.56\cdot10^{-11}$	$1.19\cdot10^{-10}$	50.6
	$7.94\cdot10^{4}$	$2.15\cdot10^{-10}$	$1.47\cdot10^{-11}$	$4.73\cdot10^{-11}$	24.1
	$1.26\cdot10^{5}$	$6.83\cdot10^{-11}$	$6.92\cdot10^{-12}$	$2.00\cdot10^{-11}$	12.3
	$2.00\cdot10^{5}$	$2.03\cdot10^{-11}$	$2.52\cdot10^{-12}$	$8.15\cdot10^{-12}$	6.0

O	$5.01•10^{3}$	$2.76•10^{-7}$	$2.64•10^{-9}$	$3.17•10^{-8}$	1969.3
	$7.94•10^{3}$	$9.64•10^{-8}$	$1.23•10^{-9}$	$1.13•10^{-8}$	1091.0
	$1.26•10^{4}$	$3.22•10^{-8}$	$5.47•10^{-10}$	$3.89•10^{-9}$	596,5
	$2.00•10^{4}$	$1.05•10^{-8}$	$2.44•10^{-10}$	$1.33•10^{-9}$	309.8
	$3.16•10^{4}$	$3.24•10^{-9}$	$9.38•10^{-11}$	$4.59•10^{-10}$	158.1
	$5.01•10^{4}$	$9.99•10^{-10}$	$4.16•10^{-11}$	$1.61•10^{-10}$	77.5
	$7.94•10^{4}$	$3.08•10^{-10}$	$1.67•10^{-11}$	$6.19•10^{-11}$	36.1
	$1.26•10^{5}$	$9.47•10^{-11}$	$7.80•10^{-12}$	$2.46•10^{-11}$	17.7
	$2.00•10^{5}$	$2.83•10^{-11}$	$2.95•10^{-12}$	$1.04•10^{-11}$	8.6
Ne	$5.01•10^{3}$	$5.01•10^{-8}$	$9.59•10^{-10}$	$6.72•10^{-9}$	374.3
	$7.94•10^{3}$	$1.83•10^{-8}$	$5.07•10^{-10}$	$2.61•10^{-9}$	215.9
	$1.26•10^{4}$	$6.32•10^{-9}$	$2.41•10^{-10}$	$1.03•10^{-9}$	121.6
	$2.00•10^{4}$	$2.19•10^{-9}$	$1.12•10^{-10}$	$3.96•10^{-10}$	66.9
	$3.16•10^{4}$	$6.96•10^{-10}$	$4.59•10^{-11}$	$1.50•10^{-10}$	35.0
	$5.01•10^{4}$	$2.21•10^{-10}$	$1.99•10^{-11}$	$6.03•10^{-11}$	17.7
	$7.94•10^{4}$	$6.84•10^{-11}$	$7.82•10^{-12}$	$2.46•10^{-11}$	8.3
	$1.26•10^{5}$	$2.37•10^{-11}$	$4.18•10^{-12}$	$1.10•10^{-11}$	4.6
	$2.00•10^{5}$	$8.21•10^{-12}$	$1.84•10^{-12}$	$4.90•10^{-12}$	2.6
Mg	$7.94•10^{3}$	$2.35•10^{-8}$	$5.80•10^{-10}$	$3.26•10^{-9}$	290.9
	$1.26•10^{4}$	$8.27•10^{-9}$	$2.63•10^{-10}$	$1.20•10^{-9}$	164.7
	$2.00•10^{4}$	$2.84•10^{-9}$	$1.26•10^{-10}$	$4.69•10^{-10}$	89.8
	$3.16•10^{4}$	$8.94•10^{-10}$	$4.99•10^{-11}$	$1.76•10^{-10}$	46.4
	$5.01•10^{4}$	$2.75•10^{-10}$	$2.23•10^{-11}$	$6.81•10^{-11}$	22.7
	$7.94•10^{4}$	$8.19•10^{-11}$	$8.37•10^{-12}$	$2.67•10^{-11}$	10.4
	$1.26•10^{5}$	$2.33•10^{-11}$	$3.41•10^{-12}$	$1.08•10^{-11}$	4.7
Si	$1.26•10^{4}$	$8.27•10^{-9}$	$2.84•10^{-10}$	$1.18•10^{-9}$	170.3
	$2.00•10^{4}$	$3.08•10^{-9}$	$1.39•10^{-10}$	$4.69•10^{-10}$	100.6
	$3.16•10^{4}$	$1.02•10^{-9}$	$5.59•10^{-11}$	$1.86•10^{-10}$	54.7
	$5.01•10^{4}$	$3.51•10^{-10}$	$2.65•10^{-11}$	$7.53•10^{-11}$	29.8
	$7.94•10^{4}$	$1.09•10^{-10}$	$1.04•10^{-11}$	$3.18•10^{-11}$	14.4
	$1.26•10^{5}$	$3.34•10^{-11}$	$4.51•10^{-12}$	$1.31•10^{-11}$	7.0
Fe	$1.26•10^{4}$	$1.86•10^{-8}$	$4.81•10^{-10}$	$2.32•10^{-9}$	385.6
	$2.00•10^{4}$	$6.55•10^{-9}$	$2.25•10^{-10}$	$8.52•10^{-10}$	215.1
	$3.16•10^{4}$	$2.05•10^{-9}$	$8.78•10^{-11}$	$2.95•10^{-10}$	107.5
	$5.01•10^{4}$	$6.56•10^{-10}$	$4.04•10^{-11}$	$1.13•10^{-10}$	54.4
	$7.94•10^{4}$	$2.02•10^{-10}$	$1.58•10^{-11}$	$4.31•10^{-11}$	26.0
	$1.26•10^{5}$	$6.02•10^{-11}$	$6.70•10^{-12}$	$1.74•10^{-11}$	12.3

	$7.94•10^{5}$	$1.05•10^{-6}$	$5.14•10^{-9}$	$1.17•10^{-7}$	7882.5
All nuclei	$1.26•10^{4}$	$3.45•10^{-7}$	$2.14•10^{-9}$	$3.88•10^{-8}$	4455.5
	$2.00•10^{4}$	$1.14•10^{-7}$	$9.58•10^{-10}$	$1.29•10^{-8}$	2356.2
	$3.16•10^{4}$	$3.54•10^{-8}$	$3.69•10^{-10}$	$4.10•10^{-9}$	1267.9
	$5.01•10^{4}$	$1.11•10^{-8}$	$1.59•10^{-10}$	$1.32•10^{-9}$	633.3
	$7.94•10^{4}$	$3.32•10^{-9}$	$5.91•10^{-11}$	$4.28•10^{-10}$	302.0
	$1.26•10^{5}$	$9.94•10^{-10}$	$2.55•10^{-11}$	$1.48•10^{-10}$	145.1
	$2.00•10^{5}$	$2.90•10^{-10}$	$9.38•10^{-12}$	$5.09•10^{-11}$	69.4
	$3.16•10^{5}$	$8.17•10^{-11}$	$3.92•10^{-12}$	$1.83•10^{-11}$	31.1
	$5.01•10^{5}$	$2.29•10^{-11}$	$1.49•10^{-12}$	$6.87•10^{-12}$	14.4
	$7.94•10^{5}$	$6.07•10^{-12}$	$6.12•10^{-13}$	$2.75•10^{-12}$	6.0